

# Isogeometric Analysis with Geometrically Continuous Functions on Planar Multi-Patch Geometries

Mario Kapl<sup>a,\*</sup>, Florian Buchegger<sup>b</sup>, Michel Bercovier<sup>c</sup>, Bert Jüttler<sup>a,b</sup>

<sup>a</sup>Radon Institute for Computational and Applied Mathematics, Austrian Academy of Sciences

<sup>b</sup>Institute of Applied Geometry, Johannes Kepler University, Linz, Austria

<sup>c</sup>The Hebrew University of Jerusalem, Israel

---

## Abstract

We generate a basis of the space of bicubic and biquartic  $C^1$ -smooth geometrically continuous isogeometric functions on bilinear multi-patch domains  $\Omega \subset \mathbb{R}^2$ . The basis functions are obtained by suitably combining  $C^1$ -smooth geometrically continuous isogeometric functions on bilinearly parameterized two-patch domains (cf. [16]). They are described by simple explicit formulas for their spline coefficients.

These  $C^1$ -smooth isogeometric functions possess potential for applications in isogeometric analysis, which is demonstrated by several examples (such as the biharmonic equation). In particular, the numerical results indicate optimal approximation power.

*Keywords:* Isogeometric Analysis,  $C^1$ -smooth isogeometric functions, geometrically continuous isogeometric functions, multi-patch domain, biharmonic equation

---

## 1. Introduction

Isogeometric Analysis (IgA) is a promising framework for performing numerical simulation, which uses the same (rational) spline function space for representing the geometry of the physical domain and describing the solution space [8, 15]. Multi-patch parameterizations have been introduced in order to perform isogeometric simulations on more complex geometries. Two main approaches for coupling the individual patches exist.

The first one does not modify the isogeometric spaces on the individual patches but uses other techniques to achieve global smoothness of the solution (at least approximately). These include the discontinuous Galerkin method [20, 27], the use of Nitsche's technique [1, 23], the mortar approach [3, 9, 12] and domain decomposition methods [13, 18]. Typically, these techniques aim at ensuring  $C^0$ -continuity weakly of the resulting numerical solution.

The second approach uses a globally defined basis for the isogeometric simulation on the multi-patch domain, thereby modifying the spaces on the individual patches and coupling

---

\*Corresponding author

*Email addresses:* `mario.kapl@ricam.oeaw.ac.at` (Mario Kapl), `florian.buchegger@jku.at` (Florian Buchegger), `berco@cs.huji.ac.il` (Michel Bercovier), `bert.juettler@jku.at` (Bert Jüttler)

them explicitly. The case of  $C^0$ -smoothness is well understood: The notion of isogeometric spline forests was introduced in [26] and was extended recently by enhancing the smoothness across interfaces and introducing hierarchical spline refinement [5]. Isogeometric function spaces possessing higher regularity, however, are more difficult to construct and require the classical notion of geometric continuity, see [24] and the references therein.

Geometric continuity is a well-established approach in Computer Aided Geometric Design for designing smooth multi-patch surfaces possessing extraordinary vertices (EVs) [10, 14], i.e., surfaces composed of quadrilateral patches where other than 4 patches may meet in some vertices. The construction of  $C^s$ -smooth isogeometric functions on multi-patch domains is based on the observation – which has been formalized firstly by Groisser and Peters [11] – that the  $C^s$ -smoothness of an isogeometric function is equivalent to the geometric smoothness of order  $s$  ( $G^s$ -smoothness) of its graph surface<sup>1</sup>, where  $s$  is a positive integer. Motivated by this we denote the  $C^s$ -smooth functions on a multi-patch domain as  *$C^s$ -smooth geometrically continuous isogeometric functions* [16].

We restrict ourselves to the case  $s = 1$ . Two different strategies following the concept of geometric smoothness have been explored.

The first one derives  $C^1$ -smooth geometrically continuous isogeometric functions from existing constructions for  $G^1$ -smooth multi-patch surfaces that originated in geometric design. Related results include the recent publications [17, 21, 22], which are based on different  $G^1$ -smooth multi-patch spline surfaces, and the use of EVs in T-spline-based representations [25]. Numerical results indicate that the accuracy of the results may deteriorate in the vicinity of the EVs. Moreover, the construction of nested isogeometric spaces via  $h$ -refinement remains an open problem if EVs are present.

The second strategy employs a basis of the entire space of  $C^1$ -smooth functions on a particular class of multi-patch geometries, cf. [2, 16], and uses it to describe the geometry and to perform isogeometric simulations. A first step was presented in [16], where we analyzed the spaces of bicubic and biquartic  $C^1$ -smooth geometrically continuous isogeometric functions on bilinearly parameterized two-patch domains. Furthermore we developed a simple framework for the construction of a basis in the general setting and obtained promising numerical results indicating optimal approximation power. These are also supported by the recent results in [7].

The approaches [2, 16] (and also the present approach) are based on *assembling* B-spline isogeometric patches. It is different from the classic higher order Finite Elements Methods (FEM) such as Clough-Tocher macro triangles and their generalization to bivariate triangular splines, cf. [19]. These FEM based approaches construct  $C^1$ -smooth bases functions per element. In contrast, the present and the earlier approaches [2, 16] deal only with the patches' interfaces and therefore the interior of each patch has the regularity of the corresponding isogeometric B-Spline (which can be higher than  $C^1$ , especially for higher order splines). Moreover, the patches can have vertices of any valence, that would not

---

<sup>1</sup>The graph surface of an isogeometric function is the 3D surface where the first two coordinates are the coordinates of the physical domain and the third coordinate is the associated value of the isogeometric function, compare Eq. (10).

be possible with classical bivariate Hermite type constructions like Bogner-Fox-Schmidt quadrilaterals, cf [6].

The present work extends the earlier results from [16], obtained for bilinearly parameterized two-patch domains, to bilinearly parameterized multi-patch domains. This generalization increases the geometric flexibility of the construction, while we also present numerical results indicating that the optimal approximation properties are preserved. We describe the construction of bicubic and biquartic  $C^1$ -smooth geometrically continuous isogeometric basis functions. The constructed basis allows the use of the same function space for performing simulation and describing the geometry in agreement with the main ideas of IgA. The basis functions are specified by simple explicit formulas for their spline coefficients in contrast to [16], where Bézier coefficients are used to present a basis of bi-degree (4, 4).

The main differences and novelties of our work compared to [2] are as follows: While our construction is based on bicubic and biquartic  $C^1$ -smooth geometrically continuous isogeometric basis functions, the work [2] mostly deals with biquintic functions and the biquartic case is only described for a specific setting of the multi-patch domain. In particular, the construction of bicubic  $C^1$ -smooth geometrically continuous isogeometric functions has not been considered at all. In [2] the basis functions are only implicitly defined by the existence of a minimal determining set for the involved Bézier coefficients. This is in contrast to our work, where the obtained functions are specified by simple explicit formulas for their spline coefficients. Furthermore, we are able to generate nested  $C^1$ -smooth isogeometric spaces which were not investigated in [2].

The paper is organized as follows. First we describe the class of bilinearly parameterized multi-patch domains  $\Omega \subset \mathbb{R}^2$ , which is considered throughout this paper, in Section 2. In addition, we introduce the spaces of bicubic and biquartic  $C^1$ -smooth geometrically continuous isogeometric functions on these domains.

The case of two-patch domains is considered in Section 3. We recall the earlier results from [16] and extend them by including explicit constructions for a basis in the bicubic case and by modifying the constructions near the boundary (both for bicubic and biquartic splines), thereby preparing the multi-patch case.

Based on these results we generate a basis of the space of  $C^1$ -smooth geometrically continuous isogeometric functions on bilinear multi-patch domains in Section 4 by suitably combining the basis functions on two-patch geometries. Finally we present several examples that demonstrate the potential of our construction for isogeometric analysis in Section 5. More precisely, we use  $C^1$ -smooth bicubic and biquartic functions for performing  $L^2$ -approximation and for solving Poisson's equation and the biharmonic equation on different multi-patch domains. The numerical results indicate optimal approximation power.

## 2. Preliminaries

The notion of  $C^s$ -smooth geometrically continuous isogeometric functions on general multi-patch domains was introduced in [16, Section 2]. In this section, we first present the particular class of bilinear multi-patch domains  $\Omega \subset \mathbb{R}^2$ , which will be considered

throughout the paper. Then we recall the concept of geometrically continuous functions for  $s = 1$ .

*Bilinear multi-patch domains.* Given a domain  $\Omega \subset \mathbb{R}^2$  with a piecewise straight boundary, we consider a quadrangulation without hanging vertices, i.e., a subdivision into mutually disjoint strictly convex quadrilaterals, which we call patches. More precisely, we assume that the quadrangulation consists of  $P \in \mathbb{Z}^+$  quadrilateral patches  $\Omega^{(\ell)}$ ,  $\ell = 1, \dots, P$ , which are joined together in  $E \in \mathbb{Z}^+$  non-boundary edges  $\Gamma^{(e)}$ ,  $e = 1, \dots, E$ . Each patch  $\Omega^{(\ell)}$  is the image of the unit square under a bilinear geometry mapping

$$\mathbf{G}^{(\ell)} : [0, 1]^2 \rightarrow \mathbb{R}^2, \quad (1)$$

represented in coordinates by

$$\boldsymbol{\xi}^{(\ell)} = (\xi_1^{(\ell)}, \xi_2^{(\ell)}) \mapsto \mathbf{G}^{(\ell)}(\boldsymbol{\xi}^{(\ell)}) = (G_1^{(\ell)}(\xi_1^{(\ell)}, \xi_2^{(\ell)}), G_2^{(\ell)}(\xi_1^{(\ell)}, \xi_2^{(\ell)})). \quad (2)$$

All these mappings are bijective and regular since the patches were assumed to be strictly convex.

*Spline bases.* We denote by  $\mathcal{S}_k^d$  the tensor-product spline space of degree  $(d, d)$ , which is defined on the unit square  $[0, 1]^2$  by choosing  $k$  uniform inner knots of multiplicity  $d - 1$  in both parameter directions. In particular, we consider degrees  $d = 3, 4$  and assume that the number of inner knots satisfies  $k \geq 5 - d$ . Each space  $\mathcal{S}_k^d$  is spanned by tensor product B-splines

$$\{N_{\mathbf{i}} : \mathbf{i} \in J\}$$

with the index set

$$J = \{\mathbf{i} = (i_1, i_2) : \mathbf{0} = (0, 0) \leq \mathbf{i} \leq (d + k(d - 1), d + k(d - 1))\}.$$

Since the bilinear geometry mappings  $\mathbf{G}^{(\ell)}$  are contained in the space  $\mathcal{S}_k^d \times \mathcal{S}_k^d$ , each geometry mapping  $\mathbf{G}^{(\ell)}$  possesses a spline representation

$$\mathbf{G}^{(\ell)}(\boldsymbol{\xi}^{(\ell)}) = \sum_{\mathbf{i} \in J} \mathbf{d}_{\mathbf{i}}^{(\ell)} N_{\mathbf{i}}(\boldsymbol{\xi}^{(\ell)}), \quad (3)$$

with spline control points  $\mathbf{d}_{\mathbf{i}}^{(\ell)} \in \mathbb{R}^2$ . The indices of all spline control points form the index space

$$I = \bigcup_{\ell \in \{1, \dots, P\}} \{\ell\} \times J.$$

In addition, we consider for each edge  $\Gamma^{(e)}$  the index space  $I_{\Gamma^{(e)}} \subseteq I$ , which is given as follows:

**Definition 1.** Let  $\Gamma^{(e)}$  be a non-boundary edge of  $\Omega$  and let  $\ell$  and  $\ell'$  be the indices of the two patches  $\Omega^{(\ell)}$  and  $\Omega^{(\ell')}$ , respectively, which possess the common edge  $\Gamma^{(e)}$ , i.e.  $\Gamma^{(e)} = \Omega^{(\ell)} \cap \Omega^{(\ell')}$ . We denote by  $I_{\Gamma^{(e)}}$  the subspace of the index space

$$\{(r, \mathbf{i}) \in I \mid r \in \{\ell, \ell'\}\},$$

which is obtained by the indices  $(r, \mathbf{i})$  whose spline control points  $\mathbf{d}_{\mathbf{i}}^{(r)}$  belong to the edge  $\Gamma^{(e)}$  or to the neighboring column of control points of the patch  $\Omega^{(r)}$ .

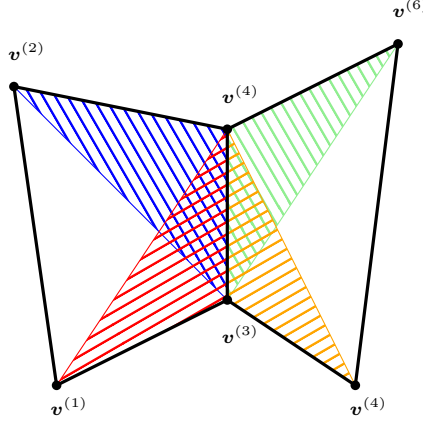


Figure 1: A two-patch subdomain is determined by 6 patch vertices  $\mathbf{v}^{(i)}$ ,  $i = 1, \dots, 6$ . The areas of the four shown triangles have to satisfy a condition, compare condition (i).

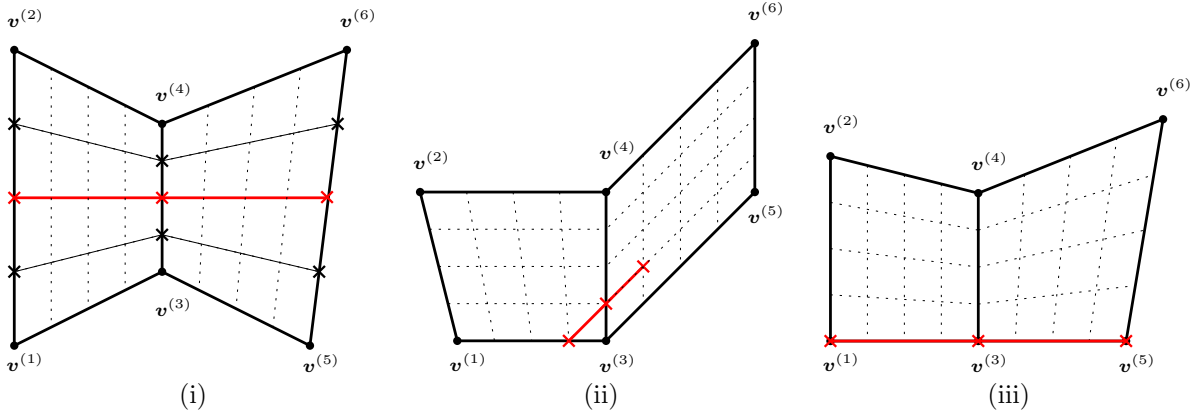


Figure 2: Two-patch subdomains violating one of the three technical conditions (i)-(iii), where the spline segments ( $k = 3$ ) are pictured as dotted lines. The crosses connected by lines are the point triplets that are assumed to be not collinear. The red color signals a violation. (It is assumed that  $\mathbf{v}^{(3)}$  is a boundary vertex of valence 3 for (ii) and an inner vertex or boundary vertex of valence other than 3 for (iii).)

*Two-patch subdomains.* Any pair of neighboring patches  $\Omega^{(\ell)}$  and  $\Omega^{(\ell')}$  defines a two-patch subdomain. We denote it by  $\Omega^{(\ell, \ell')}$  and the common edge by  $\Gamma^{(\ell, \ell')}$ . We may assume that the common boundary edge is represented by  $\mathbf{G}^{(\ell)}(1, \xi_2) = \mathbf{G}^{(\ell')}(0, \xi_2)$ . If this assumption is violated (e.g., if the edge is traced in reverse directions), we may apply a simple linear reparameterization to obtain a situation where it is satisfied.

We denote the six vertices of the two-patch subdomain as

$$\begin{aligned} \mathbf{v}^{(1)} &= \mathbf{G}^{(\ell)}(0, 0), & \mathbf{v}^{(2)} &= \mathbf{G}^{(\ell)}(0, 1), & \mathbf{v}^{(3)} &= \mathbf{G}^{(\ell)}(1, 0), \\ \mathbf{v}^{(4)} &= \mathbf{G}^{(\ell)}(1, 1), & \mathbf{v}^{(5)} &= \mathbf{G}^{(\ell')}(1, 0), & \text{and } \mathbf{v}^{(6)} &= \mathbf{G}^{(\ell')}(1, 1), \end{aligned}$$

see Fig. 1.

Recall that the dimension of the space of geometrically continuous isogeometric functions is strongly dependent on the specific geometric configuration, see [16, Table 1]. More precisely, we obtain the same dimension for all “generic” configurations, but the dimension

increases for certain special configurations. In addition, the specific construction of a basis is also dependent on the geometric configuration. A detailed investigation of the various special cases is beyond the scope of our work, see [2] for a similar discussion.

Instead we will assume three *technical conditions* (i-iii), which need to be satisfied by all two-patch subdomains. The first condition (i) ensures that dimension of the spline space on the two-patch domain is covered by the results in [16]. The remaining two conditions, which ensure that specific point triplets in the vicinity of a boundary or inner vertex are not colinear, are required for the specific construction of the basis functions.

(i) The areas of the four triangles shown in Fig. 1 satisfy

$$\text{area}(\Delta \mathbf{v}^{(3)} \mathbf{v}^{(4)} \mathbf{v}^{(1)}) \text{area}(\Delta \mathbf{v}^{(4)} \mathbf{v}^{(3)} \mathbf{v}^{(6)}) \neq \text{area}(\Delta \mathbf{v}^{(3)} \mathbf{v}^{(4)} \mathbf{v}^{(2)}) \text{area}(\Delta \mathbf{v}^{(4)} \mathbf{v}^{(3)} \mathbf{v}^{(5)}),$$

and the  $k$  point triplets

$$(1 - \xi_2) \mathbf{v}^{(1)} + \xi_2 \mathbf{v}^{(2)}, \quad (1 - \xi_2) \mathbf{v}^{(3)} + \xi_2 \mathbf{v}^{(4)}, \quad (1 - \xi_2) \mathbf{v}^{(5)} + \xi_2 \mathbf{v}^{(6)}$$

for  $\xi_2 = \frac{1}{k+1}, \frac{2}{k+1}, \dots, \frac{k}{k+1}$  are not collinear, where  $k$  specifies the number of inner knots used for defining the spline space  $\mathcal{S}_k^d$ , see Fig. 2 (left). The first assumption is equivalent to the so-called genericity condition (cf. [16, Eq. (10)]).

(ii) The point triplet

$$\frac{k}{k+1} \mathbf{v}^{(3)} + \frac{1}{k+1} \mathbf{v}^{(4)}, \quad \frac{k}{k+1} \mathbf{v}^{(3)} + \frac{1}{k+1} \mathbf{v}^{(1)} \quad \text{and} \\ \left(\frac{k}{k+1}\right)^2 \mathbf{v}^{(3)} + \frac{k}{(k+1)^2} (\mathbf{v}^{(4)} + \mathbf{v}^{(5)}) + \left(\frac{1}{k+1}\right)^2 \mathbf{v}^{(6)}$$

is not collinear if  $\mathbf{v}^{(3)}$  is a boundary vertex of valence 3, compare Fig. 2 (center). An analogous condition is required for  $\mathbf{v}^{(4)}$ .

(iii) The point triplet

$$\mathbf{v}^{(1)}, \quad \mathbf{v}^{(3)}, \quad \mathbf{v}^{(5)}$$

is not collinear if  $\mathbf{v}^{(3)}$  is an inner vertex or a boundary vertex of valence other than three, see Fig. 2 (right). An analogous condition is required for  $\mathbf{v}^{(4)}$ .

Examples of two-patch domains, which violate one of these three conditions, are visualized in Fig. 2.

*Isogeometric functions.* We consider the space  $\tilde{V}$  of isogeometric functions on the multi-patch domain  $\Omega$ ,

$$\tilde{V} = \left\{ v \in L^2(\Omega) : v|_{\Omega^{(\ell)}} \in \mathcal{S}_k^d \circ (\mathbf{G}^{(\ell)})^{-1} \text{ for } \ell = 1, \dots, P \right\}. \quad (4)$$

An isogeometric function  $w \in \tilde{V}$  is represented on each patch  $\Omega^{(\ell)}$  by

$$w(\mathbf{x}) = \left( W^{(\ell)} \circ (\mathbf{G}^{(\ell)})^{-1} \right) (\mathbf{x}), \quad \mathbf{x} \in \Omega^{(\ell)}, \quad (5)$$

with the spline function

$$W^{(\ell)}(\boldsymbol{\xi}^{(\ell)}) = \sum_{i \in J} b_i^{(\ell)} N_i(\boldsymbol{\xi}^{(\ell)}), \quad (6)$$

which is specified by coefficients  $\mathbf{b} = (b_i^{(\ell)})_{(\ell,i) \in I} \in \mathbb{R}^{|I|}$ . It can be rewritten simply as

$$w(\mathbf{x}) = \mathbf{B}(\mathbf{x})\mathbf{b}, \quad \mathbf{x} \in \Omega, \quad (7)$$

where the row vector  $\mathbf{B}$  collects the transformed B-splines

$$\mathbf{B}(\mathbf{x}) = (B_i^{(\ell)}(\mathbf{x}))_{(\ell,i) \in I} \quad (8)$$

with

$$B_i^{(\ell)}(\mathbf{x}) = \begin{cases} (N_i \circ (\mathbf{G}^{(\ell)})^{-1})(\mathbf{x}) & \text{if } \mathbf{x} \in \Omega^{(\ell)}, \\ 0 & \text{otherwise.} \end{cases} \quad (9)$$

In the sequel we will shortly write  $w = \mathbf{B}\mathbf{b}$ .

The associated graph surface  $\mathbf{F}^{(\ell)}$  has the parametric representation

$$\mathbf{F}^{(\ell)}(\boldsymbol{\xi}^{(\ell)}) = \left( \underbrace{G_1^{(\ell)}(\boldsymbol{\xi}^{(\ell)}), G_2^{(\ell)}(\boldsymbol{\xi}^{(\ell)})}_{=\mathbf{G}^{(\ell)}(\boldsymbol{\xi}^{(\ell)})}, W^{(\ell)}(\boldsymbol{\xi}^{(\ell)}) \right)^T, \quad \boldsymbol{\xi}^{(\ell)} \in [0, 1]^2. \quad (10)$$

For a function  $\mathbf{B}\mathbf{b} \in \tilde{V}$ , we denote by  $\text{supp}^*(\mathbf{b}) \subseteq I$  the support of  $\mathbf{B}\mathbf{b}$  in the spline coefficient space, i.e.,

$$\text{supp}^*(\mathbf{b}) = \{(\ell, \mathbf{i}) \in I \mid b_{\mathbf{i}}^{(\ell)} \neq 0\}.$$

*Geometrically continuous functions.* We are interested in the space

$$V = \tilde{V} \cap C^1(\Omega) = \left\{ v \in C^1(\Omega) : v|_{\Omega^{(\ell)}} \in \mathcal{S}_k^d \circ (\mathbf{G}^{(\ell)})^{-1} \text{ for } \ell = 1, \dots, P \right\}, \quad (11)$$

that contains the globally  $C^1$ -smooth isogeometric functions defined on the multi-patch domain  $\Omega$ . These functions can be characterized using the concept of geometric continuity ( $G^1$ -smoothness), see [11, Theorem 1] and [16, Theorem 1]. More precisely, the isogeometric function  $w \in \tilde{V}$  belongs to the space  $V$  if and only if for all neighboring patches  $\Omega^{(\ell)}$  and  $\Omega^{(\ell')}$ ,  $\ell, \ell' \in \{1, \dots, P\}$  with  $\ell \neq \ell'$ , the associated graph surfaces  $\mathbf{F}^{(\ell)}$  and  $\mathbf{F}^{(\ell')}$  meet with  $G^1$ -smoothness along the common edge  $\Gamma^{(\ell, \ell')}$ . This equivalence result motivated us to denote the elements of the space  $V$  as  *$C^1$ -smooth geometrically continuous isogeometric functions*.

A general framework for the construction of  $C^1$ -smooth geometrically continuous functions was described in [16, Section 2.3]. Imposing the  $G^1$ -smoothness between the graph surfaces of all neighboring patches  $\Omega^{(\ell)}$ ,  $\Omega^{(\ell')}$ ,  $\ell, \ell' \in \{1, \dots, P\}$  with  $\ell \neq \ell'$  leads to linear constraints on the spline coefficients  $b_{\mathbf{i}}^{(\ell)}$ . These form a homogeneous linear system

$$H\mathbf{b} = 0, \quad \mathbf{b} = (b_{\mathbf{i}}^{(\ell)})_{(\ell, \mathbf{i}) \in I}. \quad (12)$$

Any basis of the nullspace of  $H$  then defines a basis of the space  $V$ .

### 3. $C^1$ -smooth functions on bilinear two-patch geometries

In this section we restrict ourselves to a two-patch domain  $\Omega = \Omega^{(1,2)}$  that satisfies Assumptions (i-ii). We recall results from [16] concerning basis functions and rewrite them in a way which is convenient for their extension to the multi-patch case. Amongst others, we present the specific basis from [16] for bi-degree (4,4) with respect to spline instead of Bézier coefficients and introduce a new similar specific basis for bi-degree (3,3). In addition, we present modified functions near to the vertices of the common interface of the two-patch domain.

#### 3.1. Patch basis functions

These functions are obtained by composing a tensor-product B-spline  $N_{\mathbf{i}}$  of one of the two patches, which has zero values and derivatives on the interface, with the inverse of the geometry mapping  $\mathbf{G}^{(\ell)}$ ,

$$\mathbf{x} \mapsto \begin{cases} (N_{\mathbf{i}} \circ (\mathbf{G}^{(\ell)})^{-1})(\mathbf{x}) & \text{if } \mathbf{x} \in \Omega^{(\ell)} \\ 0 & \text{otherwise} \end{cases} \quad (\ell, \mathbf{i}) \in I \setminus I_{\Gamma^{(1,2)}}. \quad (13)$$

The support of each function is contained in only one of the two patches  $\Omega^{(1)}$  and  $\Omega^{(2)}$  and the coefficient support consists of a single index. The associated coefficient takes the value one. All coefficients with indices in  $I_{\Gamma^{(1,2)}}$  are equal to zero. The number of these functions is

$$2(d-1+k(d-1))(d+1+k(d-1)). \quad (14)$$

#### 3.2. Edge functions

These functions possess a support that is contained in both patches  $\Omega^{(1)}$  and  $\Omega^{(2)}$ , where  $\text{supp}^*(\mathbf{b})$  contains only indices  $(\ell, \mathbf{i}) \in I_{\Gamma^{(1,2)}}$ . In contrast to the patch basis functions, the associated spline coefficients  $b_{\mathbf{i}}^{(\ell)}$  of the edge functions depend on the geometry mappings. We present different types of edge functions which will be used in the next section to construct a basis of the space of  $C^1$ -smooth geometrically continuous functions on multi-patch domains. The spline coefficients of the different edge functions are computed by simple explicit formulas (see Appendix B) with respect to a corresponding local geometry (see Fig. 3), which has been introduced to substantially simplify these formulas.

*Local coordinate system.* The support in coefficient space of the constructed edge functions will be contained in at most four pairs of adjacent spline elements. For this we introduce for two, three and four pairs of adjacent spline elements (which are bilinear elements) local coordinate systems visualized in Fig. 3. These local geometries are obtained as follows: We transform  $n \in \{2, 3, 4\}$  pairs of adjacent bilinear elements in such a way that the lower and upper common vertex of the bilinear elements, i.e.

$$\mathbf{G}^{(1)}\left(1, \frac{i}{k+1}\right) \text{ and } \mathbf{G}^{(1)}\left(1, \frac{i+n}{k+1}\right),$$

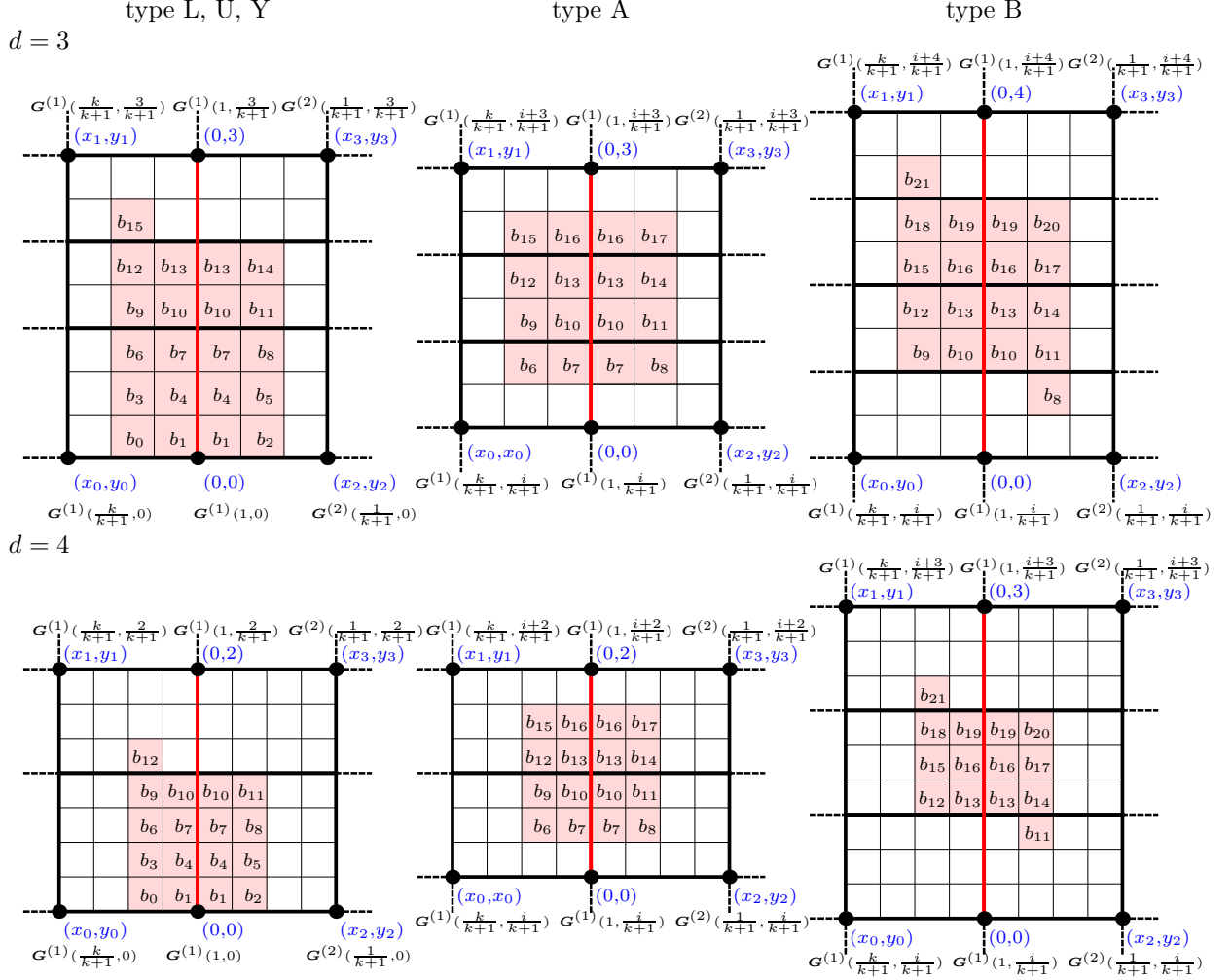


Figure 3: Support in coefficient space of the edge basis functions of type A, B, L, U, and Y for  $d = 3, 4$  on a two-patch domain  $\Omega^{(1,2)}$ , where the red edge is aligned with the interface  $\Gamma^{(1,2)}$ . The vertices of the spline elements (i.e.  $\mathbf{G}^{(\ell)}(\cdot, \cdot)$ ,  $\ell = 1, 2$ ) are transformed into local coordinates, shown in blue. These local coordinate system is used to compute the spline coefficients in Appendix B.

possess the coordinates  $(0, 0)$  and  $(0, n)$ , respectively. The remaining four vertices of the bilinear elements, i.e.

$$\mathbf{G}^{(1)}\left(\frac{k}{k+1}, \frac{i}{k+1}\right), \quad \mathbf{G}^{(1)}\left(\frac{k}{k+1}, \frac{i+n}{k+1}\right), \quad \mathbf{G}^{(2)}\left(\frac{1}{k+1}, \frac{i}{k+1}\right) \text{ and } \mathbf{G}^{(2)}\left(\frac{1}{k+1}, \frac{i+n}{k+1}\right),$$

are then transformed into coordinates  $(x_j, y_j)$ ,  $j = 1, \dots, 4$ .

These local coordinate systems are similar to the corresponding systems in [16, Fig.5], which have been introduced for the computation of the Bézier coefficients of the edge functions (see [16, Appendix]). We decided to use spline instead of Bézier coefficients to obtain a more compact representation of the edge functions. Note that a simple linear relation (cf. [14, Section 10.1.3]) allows to switch between both representations.

*Previous results.* In [16] the space of edge functions for  $d = 3, 4$  has been investigated. It has been shown that the dimension of the space is equal to

$$(2d + 1) + (2d - 4)k, \quad (15)$$

see [16, Lemma 3 and Theorem 4]. The dimension formula (15) is also valid for  $d = 2$ . Then the resulting dimension is 5, for any  $k$ , which implies that there does not exist a construction having locally supported functions and allowing  $h$ -refinement.

In addition, a specific basis of edge functions has been presented for  $d = 4$  (see [16, Section 3.3 and Appendix]). The basis consists of functions of four different types (A,B,L,U) with possible subtypes, which are locally supported on one to three pairs of adjacent spline elements. The different edge functions are described by means of simple explicit formulas for their Bézier coefficients with respect to the local coordinate system in [16, Fig.5].

In the following we recall these basis functions in detail by rewriting them with respect to their spline coefficients and present analogous basis functions for  $d = 3$ .

*Edge functions for  $d = 3$ .* The dimension of the space of edge functions is equal to  $7 + 2k$ , see Eq. (15). A specific basis consists of four types of functions, where some of them have several subtypes. Their support in coefficient space is shown in Fig. 3, top row. The values of the coefficients are specified in Appendix B.

- A: Any three consecutive pairs of adjacent spline elements (one from each subdomain) along the interface contribute one function of this type (Fig. 3, top row, center column and Eq. (B.1)). In total we have  $k - 1$  functions of this type.
- B: Any four consecutive pairs of adjacent spline elements along the interface contribute one function of this type (Fig. 3, top row, right column and Eq. (B.2)). In total we have  $k - 2$  functions of this type.
- L: These 5 functions, one for each subtype  $L_1$ - $L_5$  (Fig. 3, top row, left column and Eqns. (B.3)–(B.7)), are associated with the lower vertex of  $\Gamma^{(1,2)}$ . Their support consists of one, two or three pairs of adjacent spline elements.
- U: These 5 functions, one for each subtypes  $U_1$ - $U_5$  (Fig. 3, top row, left column and Eqns. (B.3)–(B.7)), are defined analogously to type L and are associated with the upper vertex of  $\Gamma^{(1,2)}$ .

It can be shown that these functions are linearly independent and span the entire space of edge functions. These functions are well-defined if Assumptions (i-ii) are satisfied.

*Edge functions for  $d = 4$ .* The dimension of the space of edge functions is equal to  $9 + 4k$ , see Eq. (15). A specific basis has already been presented in [16, Section 3.3 and Appendix] consisting of four types with some subtypes. We rewrite these functions in a more compact way using spline (instead of Bézier) coefficients. Their support in coefficient space is shown in Fig. 3, bottom row. The values of the coefficients are specified in Appendix B.

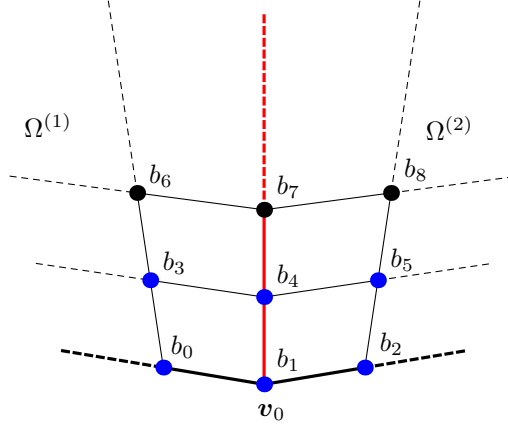


Figure 4: The 6 values  $b_i$ ,  $i = 0, \dots, 5$ , of the spline coefficients (blue vertices) of the two-patch domain  $\Omega^{(1,2)}$ , which correspond to the lower/upper vertex  $\mathbf{v}_0$  or to one-ring neighborhood of  $\mathbf{v}_0$ . (Here, the spline coefficients along the common edge (red edge) are drawn only once for both patches, since their values are equal.)

- A: Any two consecutive pairs of adjacent spline elements along the interface contribute one function of this type (Fig. 3, bottom row, center column and Eqns. (B.8)–(B.10)). In total we have  $3k$  functions of this type.
- B: Any three consecutive pairs of adjacent spline elements along the interface contribute one function of this type (Fig. 3, bottom row, right column and Eq. (B.11)). In total we have  $k - 1$  functions of this type.
- L: These 5 functions, one for each subtype  $L_1$ – $L_5$  (Fig. 3, bottom row, left column and Eqns. (B.12)–(B.16)), are associated with the lower vertex of  $\Gamma^{(1,2)}$ . Their support consists of one, two or three pairs of adjacent spline elements.
- U: These 5 functions, one for each subtype  $U_1$ – $U_5$  (Fig. 3, top row, left column and Eqns. (B.12)–(B.16)), are defined analogously to type L and are associated with the upper vertex of  $\Gamma^{(1,2)}$ .

As for  $d = 3$ , these functions are well-defined if Assumptions (i-ii) are satisfied. The graphs of the different types of functions are visualized in [16, Fig.6].

*Modified edge functions at vertices.* In order to construct a basis for the full multi-patch case, which will be discussed in the next section, we consider a new type of edge functions at the lower vertex  $\mathbf{v}_0$  (and similarly for the upper vertex). These new edge functions will be needed instead of the functions of type L (and U) in the vicinity of an inner vertex or an boundary vertex of valence greater than three, compare Section 4.3 and 4.4. We consider the six coefficients  $b_i$ ,  $i = 0, \dots, 5$ , in Fig. 3, left column, see also Fig. 4. We construct five new edge functions (type Y with subtypes  $Y_1$ – $Y_5$ ) that possess the following coefficients:

- $Y_1$ :  $b_0 = 1$ ,  $b_1 = 1$ ,  $b_2 = 1$ ,  $b_3 = 0$ ,  $b_4 = 1$ ,  $b_5 = 0$ . This function takes the value 1 at the vertex  $\mathbf{v}_0$  and possesses a vanishing gradient there.

Y<sub>2</sub>:  $b_1 = 0, b_3 = 0, b_5 = 0$ . The remaining values  $b_0, b_2$  and  $b_4$  are obtained by satisfying the conditions  $w(\mathbf{v}_0) = 0$  and  $\nabla w(\mathbf{v}_0) = (1, 0)^T$  with respect to the global coordinates.

Y<sub>3</sub>:  $b_1 = 0, b_3 = 0, b_5 = 0$ . The remaining values  $b_0, b_2$  and  $b_4$  are obtained by satisfying the conditions  $w(\mathbf{v}_0) = 0$  and  $\nabla w(\mathbf{v}_0) = (0, 1)^T$  with respect to the global coordinates.

Y<sub>4</sub>:  $b_0 = 0, b_1 = 0, b_2 = 0, b_3 = 1, b_4 = 0, b_5 = 0$ .

Y<sub>5</sub>:  $b_0 = 0, b_1 = 0, b_2 = 0, b_3 = 0, b_4 = 0, b_5 = 1$ .

The coefficients of these new functions are defined as linear combinations of the functions of type L, see Eqns. (B.17)–(B.21). Note that these functions are well-defined if Assumption (ii) is violated, provided that the Assumption (iii) is satisfied. Clearly, if the Assumptions (i-iii) are all satisfied, then the functions of type Y span the same space as the functions of type L. An analogous construction is applied at the upper vertex, and we use the same symbols to denote the resulting functions.

#### 4. $C^1$ -smooth functions on bilinear multi-patch geometries

We use the previously constructed functions on two-patch domains to generate a basis of the space  $V$ , which is formed by the  $C^1$ -smooth isogeometric functions on a given piecewise bilinear multi-patch domain.

##### 4.1. Extending the basis functions from the two-patch case

Recall that the spline coefficients  $\mathbf{b}$  define the isogeometric function  $\mathbf{B}\mathbf{b}$ , see Eq. (7). We use upper indices to denote the functions defined on two-patch subdomains, which were constructed in the previous section. More precisely, the coefficient vectors  $\mathbf{b}^{(\ell, \ell')}$  define  $C^1$ -smooth isogeometric functions  $\mathbf{B}^{(\ell, \ell')} \mathbf{b}^{(\ell, \ell')}$  on the bilinear two-patch subdomain  $\Omega^{(\ell, \ell')}$ , where  $\mathbf{B}^{(\ell, \ell')}$  is the corresponding sub-vector of the “full” vector of basis functions  $\mathbf{B}$ , see (8).

We now extend these functions to the entire multi-patch domain  $\Omega$ , simply by setting all spline coefficients  $b_i^{(r)}$  of the additional patches  $\Omega^{(r)}$ ,  $r \in \{1, \dots, P\} \setminus \{\ell, \ell'\}$ , to zero. This is done by applying the extension operator  $X^{(\ell, \ell')}$ :

**Definition 2.** Consider the spline coefficient vector  $\mathbf{b}^{(\ell, \ell')} = (\bar{b}_i^{(r)})_{r \in \{\ell, \ell'\}, i \in J}$  of the isogeometric function  $\mathbf{B}^{(\ell, \ell')} \mathbf{b}^{(\ell, \ell')}$  on the two-patch subdomain  $\Omega^{(\ell, \ell')}$ . The *extension operator*  $X^{(\ell, \ell')}$  generates the spline coefficient vector  $X^{(\ell, \ell')} \mathbf{b}^{(\ell, \ell')} = \mathbf{b} = (b_i^{(r)})_{(r, i) \in I}$  with the elements

$$b_i^{(r)} = \begin{cases} \bar{b}_i^{(r)} & \text{if } r \in \{\ell, \ell'\} \\ 0 & \text{otherwise.} \end{cases}$$

Clearly, the extended coefficient vectors define extended isogeometric functions. Some of them inherit the  $C^1$  smoothness:

**Lemma 1.** *The extended function  $\mathbf{B}X^{(\ell,\ell')}\mathbf{b}^{(\ell,\ell')}$  is  $C^1$ -smooth on  $\Omega$  if the isogeometric function  $\mathbf{B}^{(\ell,\ell')}\mathbf{b}^{(\ell,\ell')}$  on the two-patch subdomain  $\Omega^{(\ell,\ell')}$  is*

- *a patch basis function satisfying  $\text{supp}^*(X^{(\ell,\ell')}\mathbf{b}^{(\ell,\ell')}) \cap \bigcup_{e \in \{1, \dots, E\}} I_{\Gamma^{(e)}} = \emptyset$ , or*
- *an edge basis function of type A or B, or*
- *an edge basis functions of type L or Y in the vicinity of a boundary vertex of valence 3 or*
- *an edge basis functions of type L or Y in the vicinity of a boundary vertex of valence other than three satisfying*

$$\forall e : \Gamma^{(e)} \neq \Gamma^{(\ell,\ell')} \implies \text{supp}^*(X^{(\ell,\ell')}\mathbf{b}^{(\ell,\ell')}) \cap I_{\Gamma^{(e)}} = \emptyset.$$

The proof of this lemma is straightforward. Clearly, these functions do not span the full space  $V$  if inner vertices or boundary vertices with a valence other than three are present. We therefore need to combine the remaining two-patch basis functions in an appropriate way.

#### 4.2. Reduced smoothness sets and piecing together isogeometric functions

**Definition 3.** The *reduced smoothness set* (RS-set for short)  $R(\mathbf{b})$  of an isogeometric function  $\mathbf{B}\mathbf{b}$  is the collection of the edges and vertices of the multi-patch domain  $\Omega$  where this function is not  $C^1$ -smooth.

Clearly, the RS-sets of the functions covered by Lemma 1 are empty. We define an operator that allows us to create new isogeometric functions by piecing together existing ones:

**Definition 4.** Consider two isogeometric functions  $\mathbf{B}\tilde{\mathbf{b}}$  and  $\mathbf{B}\hat{\mathbf{b}}$  with coefficient vectors  $\tilde{\mathbf{b}} = (\tilde{b}_i^{(\ell)})_{(\ell,i) \in I}$  and  $\hat{\mathbf{b}} = (\hat{b}_i^{(\ell)})_{(\ell,i) \in I}$ , respectively. We assume that all corresponding pairs of non-zero spline coefficients are identical, i.e.,

$$\hat{b}_i^{(\ell)} \neq \tilde{b}_i^{(\ell)} \implies \hat{b}_i^{(\ell)}\tilde{b}_i^{(\ell)} = 0.$$

The operator  $\oplus$ , which pieces together these two functions, generates the isogeometric function  $\mathbf{B}\mathbf{b}$  with coefficients  $\mathbf{b} = \tilde{\mathbf{b}} \oplus \hat{\mathbf{b}}$  defined by

$$b_i^{(\ell)} = \begin{cases} \tilde{b}_i^{(\ell)} & \text{if } \hat{b}_i^{(\ell)} = 0, \\ \hat{b}_i^{(\ell)} & \text{if } \tilde{b}_i^{(\ell)} = 0, \\ \tilde{b}_i^{(\ell)} & \text{if } \tilde{b}_i^{(\ell)} = \hat{b}_i^{(\ell)}. \end{cases}$$

This operation is commutative and associative and will be used to obtain isogeometric functions with smaller RS-sets:

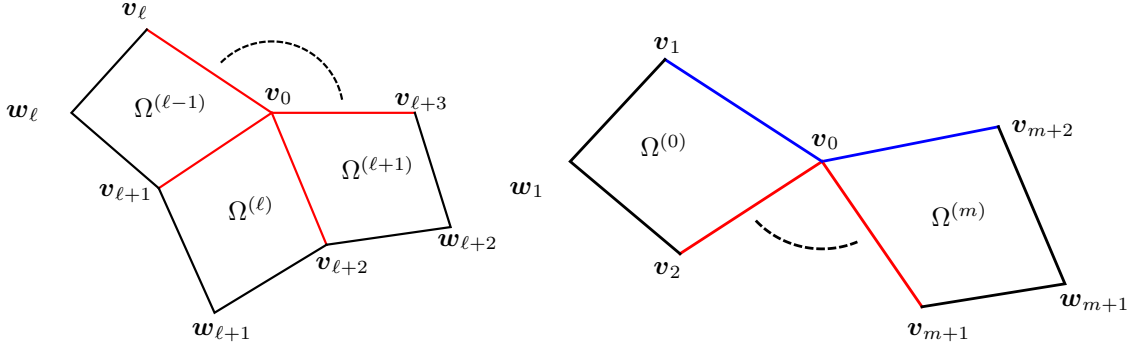


Figure 5: Left: An inner vertex  $\mathbf{v}_0$  of valence  $m \geq 3$  with the  $m$  neighboring patches  $\Omega^{(\ell)}$  in counterclockwise order around the vertex  $\mathbf{v}_0$ . Right: A boundary vertex  $\mathbf{v}_0$  of valence  $m + 2$  with  $m \geq 2$ , where the  $m + 1$  neighboring patches  $\Omega^{(\ell)}$  are ordered counterclockwise around the vertex  $\mathbf{v}_0$ . Both: The red edges are the common edges between two neighboring patches, and the blue edges are boundary edges of the multi-patch domain  $\Omega$ .

**Lemma 2.** *We consider the situation described in Definition 4, and we select an edge  $\Gamma^{(e)}$  that belongs to the RS-set  $R(\tilde{\mathbf{b}})$  of  $\mathbf{B}\tilde{\mathbf{b}}$  but not to the RS-set  $R(\hat{\mathbf{b}})$  of  $\mathbf{B}\hat{\mathbf{b}}$ . This edge is not contained in the RS-set  $R(\hat{\mathbf{b}} \oplus \tilde{\mathbf{b}})$  of the isogeometric function  $\mathbf{B}(\hat{\mathbf{b}} \oplus \tilde{\mathbf{b}})$  if the coefficient supports satisfy*

$$(\text{supp}^*(\tilde{\mathbf{b}}) \cap I_{\Gamma^{(e)}}) \subseteq (\text{supp}^*(\hat{\mathbf{b}}) \cap I_{\Gamma^{(e)}}).$$

*Proof.* According to Definition 4, the spline coefficients  $b_i^{(\ell)}$  coincide with the spline coefficients  $\hat{b}_i^{(\ell)}$  for all  $(\ell, i) \in I_{\Gamma^{(e)}}$ . Since the function  $\mathbf{B}\hat{\mathbf{b}}$  is  $C^1$ -smooth across  $\Gamma^{(e)}$ , this property is inherited by  $\mathbf{B}(\hat{\mathbf{b}} \oplus \tilde{\mathbf{b}})$ .  $\square$

#### 4.3. Vertex basis functions

We first describe the construction of  $C^1$ -smooth basis functions in the vicinity of inner vertices. In the second part of this section we will adapt it to the case of boundary vertices of valence other than three. For both cases, the resulting  $C^1$ -smooth functions will be denoted as *vertex basis functions*.

*Inner vertex.* We consider an inner vertex  $\mathbf{v}_0$  of valence  $m \geq 3$ , and assume that the  $m$  neighboring patches  $\Omega^{(\ell)}$ ,  $\ell = 0, \dots, m - 1$ , are given in a clockwise order around the vertex  $\mathbf{v}_0$ , see Fig. 5 (left). All upper indices in this paragraph will be considered modulo  $m$ .

We denote by  $\mathbf{y}_i^{(\ell, \ell+1)}$  the spline coefficient vector of the edge basis function of type  $Y_i$  for the two-patch subdomain  $\Omega^{(\ell, \ell+1)}$ . The extended functions  $\mathbf{B}X^{(\ell, \ell+1)}\mathbf{y}_i^{(\ell, \ell+1)}$  possess the RS-sets

$$R(X^{(\ell, \ell+1)}\mathbf{y}_i^{(\ell, \ell+1)}) = \{\mathbf{v}_0, \Gamma^{(\ell-1, \ell)}, \Gamma^{(\ell+1, \ell+2)}\}, \quad i = 1, 2, 3, \quad (16)$$

and

$$R(X^{(\ell, \ell+1)}\mathbf{y}_4^{(\ell, \ell+1)}) = \{\Gamma^{(\ell+1, \ell+2)}\}, \quad R(X^{(\ell, \ell+1)}\mathbf{y}_5^{(\ell, \ell+1)}) = \{\Gamma^{(\ell-1, \ell)}\}. \quad (17)$$

We define 3 proper vertex basis functions,

$$\mathbf{B}\left(\bigoplus_{\ell=0}^{m-1} X^{(\ell, \ell+1)}\mathbf{y}_i^{(\ell, \ell+1)}\right), \quad i = 1, 2, 3. \quad (18)$$

These functions are  $C^1$ -smooth on  $\Omega$ , since their RS-sets are empty. Indeed, piecing together the first  $j + 1$  functions in (18) gives the RS sets

$$R\left(\bigoplus_{\ell=0}^j X^{(\ell,\ell+1)} \mathbf{y}_i^{(\ell,\ell+1)}\right) = \{\mathbf{v}_0, \Gamma^{(-1,0)}, \Gamma^{(j+1,j+2)}\}, \quad j = 0, \dots, m-2. \quad (19)$$

This is confirmed easily with the help of Lemma 2. Note that the RS set for  $j = m - 2$  contains only the edge  $\Gamma^{(-1,0)} = \Gamma^{(m-1,m)}$  and the vertex  $\mathbf{v}_0$ . Finally, adding the last extended edge function produces a  $C^1$ -smooth function since

$$R\left(\bigoplus_{\ell=0}^{m-1} X^{(\ell,\ell+1)} \mathbf{y}_i^{(\ell,\ell+1)}\right) = \emptyset. \quad (20)$$

The remaining edge is eliminated according to Lemma 2 and the vertex  $\mathbf{v}_0$  is not contained in the RS-set anymore since the gradient of the resulting function takes the values  $(0, 0)$ ,  $(1, 0)$  and  $(0, 1)$  at  $\mathbf{v}_0$  for  $i = 1, 2$  and  $3$ , respectively.

In addition to the proper vertex functions, we define  $m$  twist vertex basis functions,

$$\mathbf{B}(X^{(\ell,\ell+1)} \mathbf{y}_4^{(\ell,\ell+1)} \oplus X^{(\ell+1,\ell+2)} \mathbf{y}_5^{(\ell+1,\ell+2)}), \quad \ell = 0, \dots, m-1. \quad (21)$$

These functions are  $C^1$ -smooth on  $\Omega$  since their RS sets are empty according to Lemma 2.

As an example, Fig. 6 shows the 8 vertex basis functions for an inner vertex  $\mathbf{v}_0$  of valence 5.

*Boundary vertex.* A slight modification of this construction is needed to obtain the vertex basis functions at a boundary vertex  $\mathbf{v}_0$  of valence  $m + 2$  with  $m \geq 2$ . We assume that the  $m + 1$  neighboring patches  $\Omega^{(\ell)}$ ,  $\ell = 0, \dots, m$ , are ordered counterclockwise around the vertex  $\mathbf{v}_0$ , see Fig. 5 (right). Again, we denote by  $\mathbf{y}_i^{(\ell,\ell+1)}$  the spline coefficient vector of the edge basis function of type  $Y_i$  for the two-patch subdomain  $\Omega^{(\ell,\ell+1)}$ .

The RS sets of the extended edge functions are the same as in (16) and (17), except for the RS sets

$$R(X^{(0,1)} \mathbf{y}_i^{(0,1)}) = \{\mathbf{v}_0, \Gamma^{(1,2)}\}, \quad R(X^{(m-1,m)} \mathbf{y}_i^{(m-1,m)}) = \{\mathbf{v}_0, \Gamma^{(m-2,m-1)}\}, \quad i = 1, 2, 3, \quad (22)$$

and

$$R(X^{(0,1)} \mathbf{y}_5^{(0,1)}) = \emptyset, \quad R(X^{(m-1,m)} \mathbf{y}_4^{(m-1,m)}) = \emptyset, \quad (23)$$

which correspond to the two-patch subdomains  $\Omega^{(0,1)}$  and  $\Omega^{(m-1,m)}$ .

We define 3 proper vertex basis functions and  $m - 2$  twist vertex basis functions for  $\ell = 1, \dots, m - 2$  as before. In addition we obtain two twist vertex basis functions, which are simply the extended functions

$$\mathbf{B}X^{(0,1)} \mathbf{y}_5^{(0,1)} \quad \text{and} \quad \mathbf{B}X^{(m-1,m)} \mathbf{y}_4^{(m-1,m)}. \quad (24)$$

All these functions are  $C^1$ -smooth on  $\Omega$ .

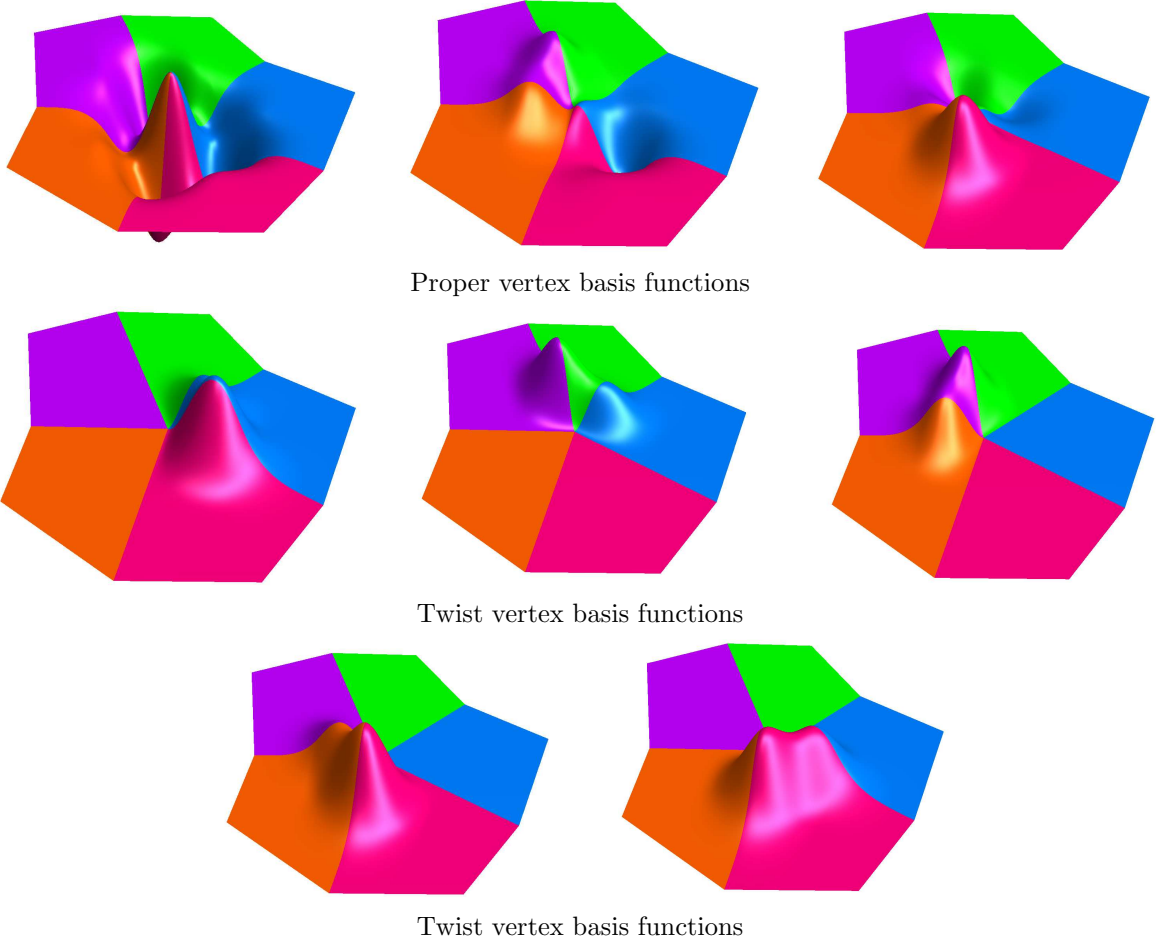


Figure 6: The 8 vertex basis functions (3 proper vertex basis functions and 5 twist vertex basis functions) at an inner vertex of valence 5 for  $d = 4$ .

#### 4.4. Basis of the space

The previous sections described the construction of different kinds of  $C^1$ -smooth geometrically continuous isogeometric functions on  $\Omega$ . We categorize these functions into four sets  $\mathcal{H}_i$  ( $i = 1, \dots, 4$ ) according to their construction.

The first set  $\mathcal{H}^1$  consists of the extended patch basis functions with only one non-zero spline coefficient  $b_i^{(\ell)}$  which satisfies that  $(\ell, i) \notin I_{\Gamma(e)}$  for  $e = 1, \dots, E$ . The number of these functions for each geometry mapping  $\mathbf{G}^{(\ell)}$ ,  $\ell = 1, \dots, P$ , depends on the number of interfaces (i.e. edges) of the patch  $\mathbf{G}^{(\ell)}$  with its neighbors. In detail, this number  $\nu^{(\ell)}$  is given by

$$\nu^{(\ell)} = \begin{cases} (d-1+k(d-1))(d+1+k(d-1)) & \text{for one interface,} \\ (d-1+k(d-1))^2 & \text{for two interfaces with a common vertex,} \\ (d-3+k(d-1))(d+1+k(d-1)) & \text{for two interfaces without a common vertex,} \\ (d-3+k(d-1))(d-1+k(d-1)) & \text{for three interfaces, and} \\ (d-3+k(d-1))^2 & \text{for four interfaces.} \end{cases}$$

The total number is obtained by summing up the individual contributions,

$$\#\mathcal{H}^1 = \sum_{\ell=1}^P \nu^{(\ell)}. \quad (25)$$

The second set  $\mathcal{H}^2$  contains the  $(2d-9) + (2d-4)k$  extended edge basis functions of type A and B for each edge  $\Gamma^{(e)}$ ,  $e = 1, \dots, E$ . Therefore,

$$\#\mathcal{H}^2 = E((2d-9) + (2d-4)k). \quad (26)$$

The next set  $\mathcal{H}^3$  contains the 5 extended edge basis functions of type L for each boundary vertex of valence three, thus

$$\#\mathcal{H}^3 = 5R, \quad (27)$$

where  $R$  is the number of different boundary vertices of valence three.

Finally, the set  $\mathcal{H}^4$  contains the  $3 + m$  vertex basis functions for each inner vertex of valence  $m \geq 3$ , and the  $3 + (m-1)$  vertex basis functions for each boundary vertex of valence  $m \geq 4$ . Therefore,

$$\#\mathcal{H}^4 = \sum_{\mathbf{v}:\text{inner vertex}} (3 + m_{\mathbf{v}}) + \sum_{\mathbf{v}:\text{boundary vertex}} (3 + m_{\mathbf{v}} - 1), \quad (28)$$

where  $m_{\mathbf{v}}$  is the valence of the vertex  $\mathbf{v}$ .

Clearly, the four sets are mutually disjoint. We consider the union  $\mathcal{H} = \cup_{i=1}^4 \mathcal{H}^i$ .

**Theorem 1.** *The functions in  $\mathcal{H}$  form a basis of the space  $V$  of  $C^1$ -smooth geometrically continuous isogeometric functions on  $\Omega$ . The dimension  $V$  is thus equal to*

$$\dim V = \sum_{i=1}^4 \#\mathcal{H}^i. \quad (29)$$

PROOF. We consider a function  $w \in V$ . It possesses a unique representation with spline coefficients  $(b_i^{(\ell)})_{(\ell, \mathbf{i}) \in I}$ . We show that this function can be represented as a linear combination of functions in  $\mathcal{H}$ . This is proved repeatedly subtracting linear combinations of functions of  $\mathcal{H}$  from the function  $w$  until the null function is obtained.

1. We consider all inner vertices and all boundary vertices of valence other than three. For each such vertex, the gradient and the value of  $w$  at the vertex determines a unique linear combination of the three proper vertex basis functions. Subtracting all these linear combinations from  $w$  creates a function  $w'$  which has zero values and gradients at these vertices.
2. Considering again the inner vertices and boundary vertices of valence other than three. For each such vertex, the spline coefficient of  $w'$  at the vertex and the first neighboring spline coefficients along edges are all zero. The remaining spline coefficients in the one-ring neighborhood correspond to the twist vertex basis functions. Subtracting a suitable linear combination of those (i.e., multiplied by the associated spline coefficients) creates a function  $w''$  which has only zero spline coefficients in the 1-ring neighborhoods of the considered vertices.

3. Now we consider all inner edges, one by one. Subtracting a suitable linear combination of edge basis functions of types A and B (plus five extended edge basis functions of type L for each boundary vertex of valence 3 if present) creates a function  $w'''$  which has only zero spline coefficients  $(\ell, \mathbf{i}) \in I_{\Gamma(e)}$ ,  $e = 1, \dots, E$ . This is guaranteed to work since these functions generate all spline coefficients of  $C^1$ -smooth isogeometric functions on two-patch domains in the vicinity of the common edge, see Section 3.2.
4. Finally we represent  $w'''$  as a linear combination of extended patch basis functions.

The linear independence of  $\mathcal{H}$  is inherited from the linear independence on two-patch domains, due to the disjoint supports in coefficient space. For the proper vertex and twist vertex functions, this is guaranteed by their construction, as they interpolate characteristic data for values, gradients, and mixed derivatives.  $\square$

Any function  $w \in V$  belongs to  $H^2(\Omega)$ , since it is globally  $C^1$ -smooth and piecewise  $C^\infty$ -smooth. Thus we may use them to solve higher order partial differential equations over multi-patch domains. This is presented in the following section.

## 5. Examples

We present examples of using  $C^1$ -smooth geometrically continuous isogeometric functions on different multi-patch domains to perform  $L^2$  approximation, to solve numerically Poisson's equation and to numerically solve the biharmonic equation. These problems have been described in some detail in [16, Section 4.2-4.4] for two-patch domains. We now consider the extension to the multi-patch case. All integrals are computed by means of Gaussian quadrature with  $(d+1)^2$  points for each spline element.

The first numerical examples (Examples 2-4) analyzes the approximation power of  $C^1$ -smooth geometrically continuous isogeometric functions on multi-patch domains. We first present the multi-patch domains which are used for solving the corresponding numerical problems in these examples.

**Example 1.** We consider three different multi-patch domains  $\Omega$ , see Fig. 7, consisting of three, four and five quadrilateral patches  $\Omega^{(\ell)}$ , respectively. The coordinates of the vertices  $\mathbf{v}_i$  of the single quadrilateral patches are presented in Appendix A. The corresponding geometry mappings  $\mathbf{G}^{(\ell)}$  of the domains  $\Omega$  are bilinear parameterizations, which are represented as Bézier patches of degree  $(d, d)$  for  $d = 3, 4$ . We perform dyadic  $h$ -refinement by considering values  $k = 2^\lambda - 1$  for suitable values of  $\lambda$ . The resulting refined geometry mappings are used to construct  $C^1$ -smooth geometrically continuous basis functions as described in the previous section. Note that this construction requires  $\lambda > 1$  for  $d = 3$  and  $\lambda > 0$  for  $d = 4$ . A different construction (not presented here) yields a basis for the remaining values of  $\lambda$ .

The resulting spaces of isogeometric basis functions are denoted by  $V_h$ , where  $h = \mathcal{O}(2^{-\lambda})$ . In addition, we denote by  $V_{0,0h}$  and  $V_{1,0h}$ , those subspaces of  $V_h$  which satisfy homogeneous boundary conditions of order 0 and 1, respectively.

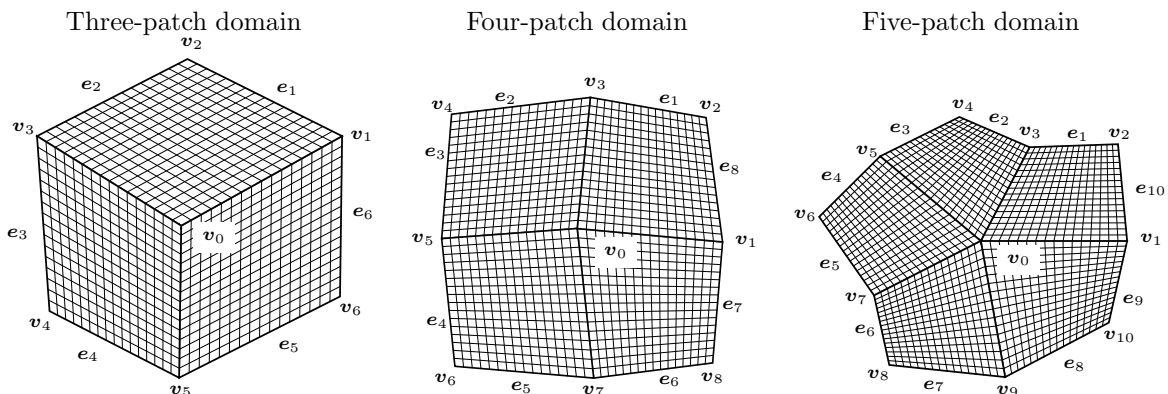


Figure 7: Computational domains  $\Omega$ , which are defined in Example 1 and Appendix A, and which are used for numerically solving various partial differential equations in the Examples 2-4.

We start with the  $L^2$  approximation of a function:

**Example 2.** We approximate the function

$$z(x_1, x_2) = 2 \cos(2x_1) \sin(2x_1), \quad (30)$$

defined on the three computational domains  $\Omega$ , shown in Fig. 7, by a function  $u_h \in V_h$  by solving the  $L^2$  minimization problem

$$\|u_h - z\|_0^2 = \int_{\Omega} (u_h(\mathbf{x}) - z(\mathbf{x}))^2 d\mathbf{x} \rightarrow \min_{u_h \in V_h}. \quad (31)$$

The detailed isogeometric formulation of the problem (31) can be found in [16, Section 4.2].

The results, reported in Fig. 8, confirm the optimal approximation order with respect to the  $H^0$  ( $L^2$ ) norm and indicate an estimated growth rate of  $\mathcal{O}(1)$  for the condition numbers of the diagonally scaled mass matrices, cf. [4].

We continue with solving Poisson's equation on the three multi-patch domains  $\Omega$  shown in Figure 7:

**Example 3.** We consider the Poisson problem

$$\begin{cases} \Delta u(\mathbf{x}) = -f(\mathbf{x}) & \text{on } \Omega \\ u(\mathbf{x}) = 0 & \text{on } \partial\Omega \end{cases} \quad (32)$$

with  $f \in H^0(\Omega)$  for the unknown function  $u \in H_0^1$ . By using the weak formulation and Galerkin projection (cf. [8]) we obtain the following problem: Find  $u_h \in V_{0,0h}$  by solving the system of equations

$$\int_{\Omega} (\nabla u_h(\mathbf{x}))^T \nabla v_h(\mathbf{x}) d\mathbf{x} = \int_{\Omega} f(\mathbf{x}) v_h(\mathbf{x}) d\mathbf{x} \quad (33)$$

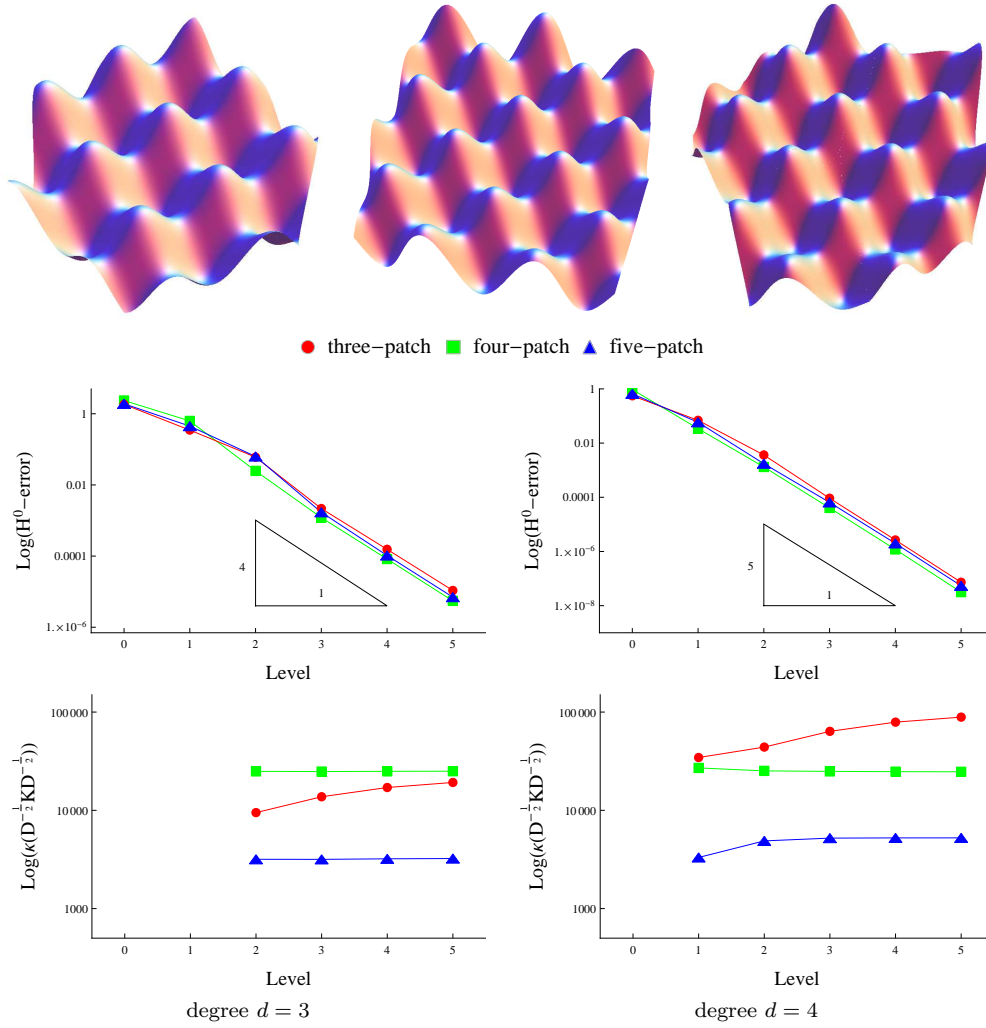


Figure 8:  $L^2$  approximation on the three computational domains shown in Fig. 7. Exact solutions (30) (top row), estimated convergence rates (center) and estimated growth of the condition numbers (bottom row). See Example 2.

for all  $v_h \in V_{0,0h}$ . The detailed isogeometric formulation of the problem (33) is presented in [16, Section 4.3].

We solve the problem (33) for the three multi-patch domains with the exact solutions

$$u(x_1, x_2) = \frac{1}{C} \prod_{i=1}^n e_i(x_1, x_2), \quad (34)$$

where  $n$  is equal to the number of boundary edges of the corresponding domain, the  $e_i$  are the linear equations of the boundary edges obtained via their Hesse normal form with outward oriented normal, and  $C$  is equal to  $0.5 \cdot 10^6$  for the three-patch domain and equal to  $10^8$  for the four- and five-patch domain. These functions  $u$ , which are visualized in Fig. 9 (top row), satisfy the homogeneous boundary conditions of order 0. The numerical results, which are reported in Fig. 9, confirm the optimal approximation order with respect to  $H^i$ -norms,  $i = 0, 1$ , and indicate an estimated growth rate of  $\mathcal{O}(h^{-2})$  for the condition numbers of the diagonally scaled system matrices, cf. [4].

We also solve the biharmonic equation on the three multi-patch domains  $\Omega$  shown in Figure 7:

**Example 4.** We consider for the unknown function  $u \in H_0^2$  the first biharmonic boundary value problem

$$\begin{cases} \Delta^2 u(\mathbf{x}) = f(\mathbf{x}) & \text{on } \Omega \\ u(\mathbf{x}) = \frac{\partial u}{\partial \mathbf{n}}(\mathbf{x}) = 0 & \text{on } \partial\Omega \end{cases} \quad (35)$$

with  $f \in H^0(\Omega)$ . Using the weak formulation and Galerkin projection (cf. [8]) leads to the problem of finding  $u_h \in V_{1,0h}$  by solving the system of equations

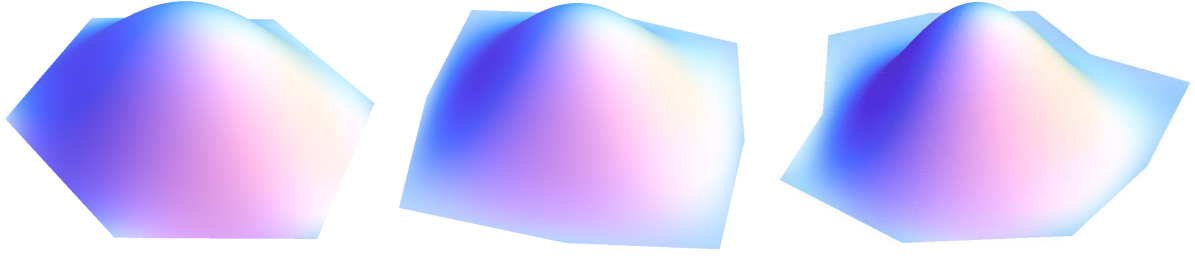
$$\int_{\Omega} \Delta u_h(\mathbf{x}) \Delta v_h(\mathbf{x}) d\mathbf{x} = \int_{\Omega} f(\mathbf{x}) v_h(\mathbf{x}) d\mathbf{x} \quad (36)$$

for all  $v_h \in V_{1,0h}$ . The detailed isogeometric formulation of the problem (36) can be found in [16, Section 4.4].

We solve the problem (36) for the three multi-patch domains with the right side functions determined by the exact solutions  $\tilde{u} = u^2$ , where  $u$  is given by (34). These functions  $\tilde{u}$  fulfill the homogeneous boundary conditions of order 1. The numerical results indicate optimal convergence rates in the  $H^i$ -norms,  $i = 0, 1, 2$ , and show an estimated growth rate of  $\mathcal{O}(h^{-4})$  for the condition numbers of the diagonally scaled system matrices (cf. [4]), see Fig. 10 and Table 1.

So far, the constructions described in this paper are limited to bilinearly parameterized multi-patch domains. Two approaches for extending the applicability have been identified in [16, Section 3.4]. We present one example for each of them:

**Example 5.** A computational domain with a hole can be modeled by four quadrilateral patches, see Fig. 11 (left). We relaxed the requirement of bilinear patches by modifying the locations of the control points that do not affect the edge and vertex basis functions. More



● three-patch    ■ four-patch    ▲ five-patch

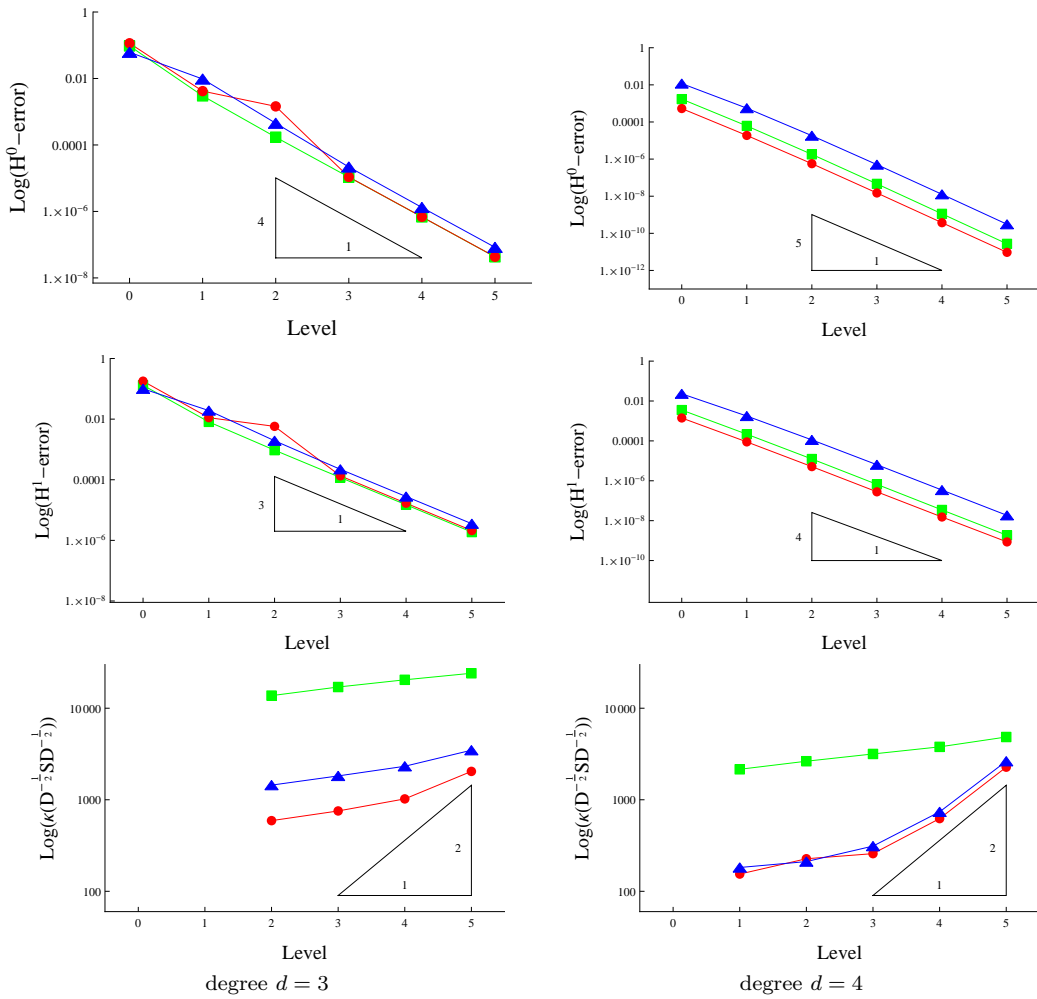


Figure 9: Solving the Poisson problem on the three computational domains shown in Fig. 7. Exact solutions (34) (top row), estimated convergence rates (second and third row) for different norms and estimated growth of the condition numbers (bottom row). See Example 3.

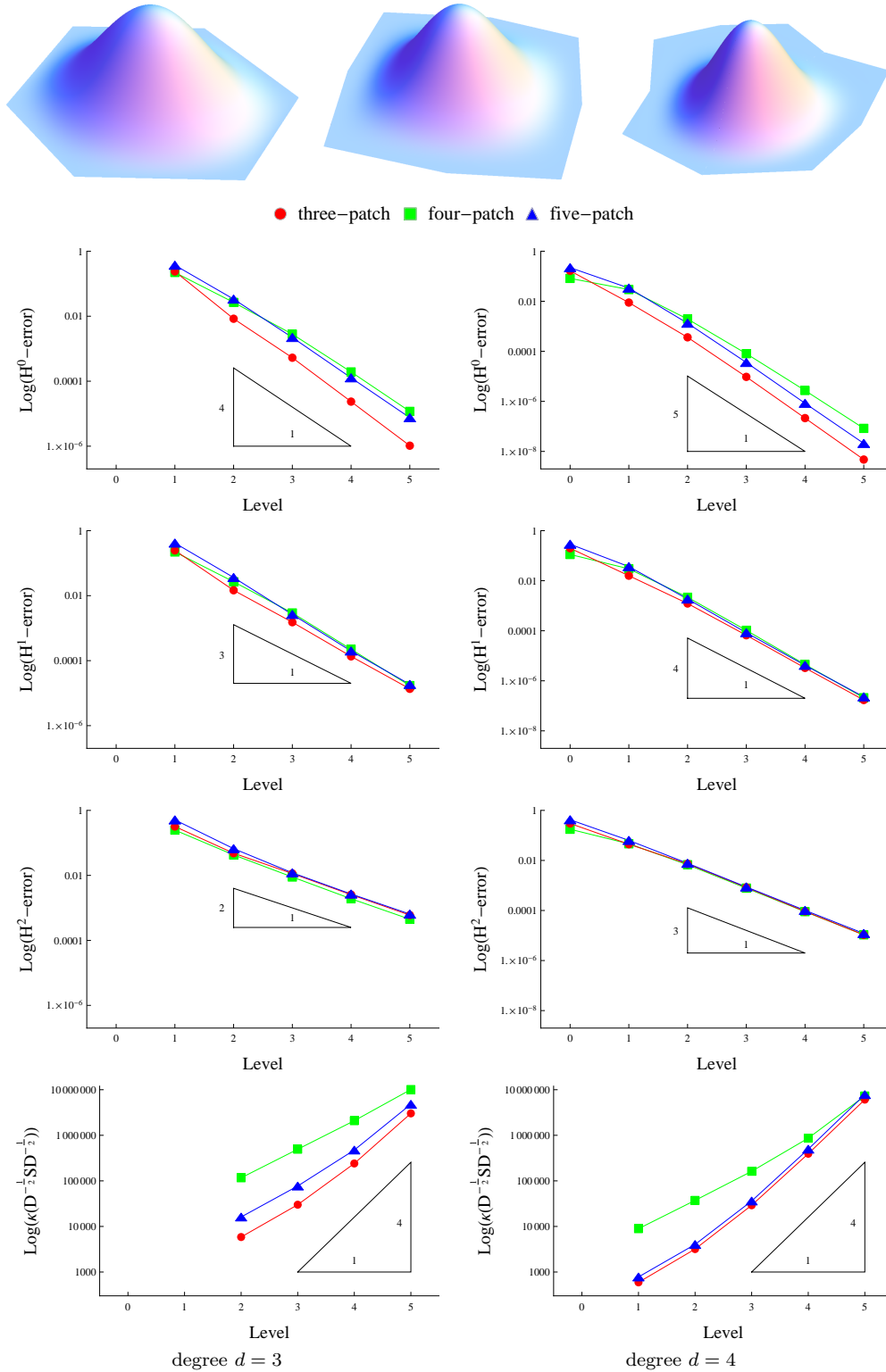


Figure 10: Solving the biharmonic equation on the three computational domains shown in Fig. 7. Exact solutions (top row), estimated convergence rates (second to fourth row) for different norms and estimated growth of the condition numbers (bottom row). See Example 4 and Table 1.

	Bicubic				Biquartic			
	e.c.r. $H^0$ -norm	e.c.r. $H^1$ -norm	e.c.r. $H^2$ -norm	rate $\kappa$	e.c.r. $H^0$ -norm	e.c.r. $H^1$ -norm	e.c.r. $H^2$ -norm	rate $\kappa$
$\lambda$	Three-patch domain							
0/1	-	-	-	-	4.21	3.64	2.75	-
1/2	4.84	4.08	2.73	-	4.61	3.69	2.61	2.43
2/3	3.99	3.27	2.08	2.36	5.25	4.21	3.13	3.19
3/4	4.49	3.49	2.16	3.01	5.47	4.34	3.19	3.74
4/5	4.51	3.32	2.09	3.65	5.5	4.26	3.12	3.95
$\lambda$	Four-patch domain							
0/1	-	-	-	-	1.48	1.9	1.93	-
1/2	3.06	3.04	2.54	-	3.91	3.78	2.79	2.06
2/3	3.25	3.19	2.26	2.08	4.6	4.39	3.1	2.12
3/4	3.86	3.71	2.22	2.08	4.89	4.53	3.12	2.42
4/5	4.03	3.72	2.09	2.27	5.03	4.42	3.08	3.08
$\lambda$	Five-patch domain							
0/1	-	-	-	-	2.71	2.98	2.74	-
1/2	3.47	3.52	2.94	-	4.67	4.3	3.04	2.37
2/3	3.92	3.78	2.47	2.26	5.21	4.47	3.14	3.17
3/4	4.12	3.73	2.17	2.62	5.42	4.33	3.11	3.78
4/5	4.08	3.41	2.05	3.34	5.33	4.19	3.07	3.98

Table 1: The estimated convergence rates (e.c.r.) in the  $H^i$ -norms,  $i = 0, 1, 2$ , and estimated growth rates for the condition numbers  $\kappa$  of the diagonally scaled system matrices by solving the biharmonic equation on three multi-patch domains in Example 4. Compare Fig.10.

precisely, the domain is modeled by considering four two-patch domains with geometric continuity across their internal interface and merging adjacent patches with standard  $C^1$ -smoothness. This allows us to construct the computational domain with a curved boundary around the hole. Slightly different to Example 3, we solve Poisson's equation with the right side function  $f$  and Dirichlet boundary conditions obtained from the exact solution

$$u(x_1, x_2) = \frac{1}{20000}(x_2 - 5)(x_2 + 4)\left(23 + \frac{9x_1}{2} - x_2\right)\left(23 - \frac{9x_1}{2} - x_2\right)(x_1^2 + x_2^2 - 2), \quad (37)$$

see Fig. 11 (right). By using biquartic functions the resulting relative  $H^0$ - and  $H^1$ -error for  $\lambda = 2$  are equal to  $8.25e-05$  and  $3.62e-04$ , respectively.

A different approach has been used in the final example:

**Example 6.** The computational domain  $\Omega$ , which is shown in Fig. 12 (bottom left), roughly resembles a car part. It has been constructed by using the second generalization described in [16, Section 3.4]. More precisely, we first consider the target geometry  $\tilde{\mathbf{G}}$  given in Fig. 12 (top right), which represents the desired car part. Thereby, the target geometry  $\tilde{\mathbf{G}}$  consists of five patches  $\tilde{\mathbf{G}}^{(\ell)} \in \mathcal{S}_3^4 \times \mathcal{S}_3^4$ . For this target geometry we choose a bilinear reference geometry  $\bar{\mathbf{G}}$ , see Fig.12 (top left), whose geometry mapping  $\bar{\mathbf{G}}$  also consists of five patches  $\bar{\mathbf{G}}^{(\ell)} \in \mathcal{S}_3^4 \times \mathcal{S}_3^4$ . The reference geometry determines a basis of the corresponding space  $\bar{V}$  of  $C^1$ -smooth geometrically continuous isogeometric functions. We then use these functions to perform  $L^2$  approximation for each coordinate function of the target geometry to obtain a parametrization  $\mathbf{G}$  of the computational domain  $\Omega$ . The obtained relative  $H^0$ -errors with respect to the two coordinates are equal to  $6.36e-04$  and  $8.89e-04$ , respectively. The geometry mapping  $\mathbf{G}$  is thus contained in the space  $\bar{V} \times \bar{V}$ . The coefficients of the associated basis functions are inherited from the reference geometry.

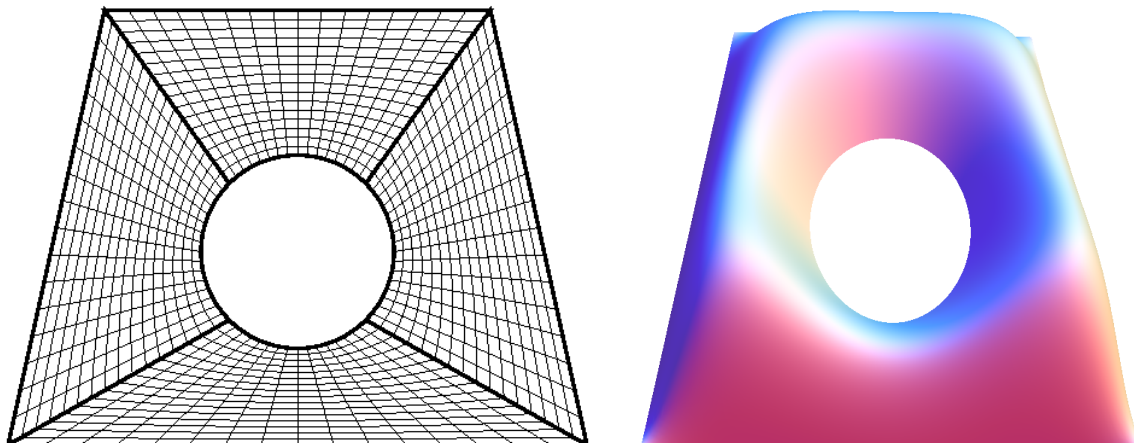


Figure 11: Solving Poisson's equation on a four-patch computational domain with hole (left) with the right side function  $f$  and Dirichlet boundary conditions determined by the exact solution (37) (right). See Example 5.

#ptchs	#fcts	rel. $H^0$ -error	e.c.r. $H^0$ -norm	rel. $H^1$ -error	e.c.r. $H^1$ -norm
80	808	1.66744e-03	-	7.30986e-03	-
320	3048	5.44177e-05	4.93741	4.68758e-04	3.96293
1280	11848	1.47709e-06	5.20324	2.91532e-05	4.00711
5120	46728	3.7166e-08	5.31263	1.66268e-06	4.13207

Table 2: The obtained relative  $H^i$ -errors,  $i = 0, 1$ , with the corresponding estimated convergence rates (e.c.r.) by solving the Poisson problem in Example 6.

We solve Poisson's equation with the right side function  $f$  and Dirichlet boundary conditions determined by the exact solution

$$u(x_1, x_2) = \frac{1}{5000} (4 - x_2) \left(4 + \frac{5x_1}{3} - x_2\right) \left(\frac{3}{2} - x_2\right) (x_1 + 5) \left(-\frac{7}{2} - x_2\right) \left(x_1^2 + \left(x_2 + \frac{7}{2}\right)^2 - 4\right) (x_1 - 5). \quad (38)$$

Table 2 shows the resulting relative  $H^i$ -errors,  $i = 0, 1$ , with the corresponding estimated convergence rates.

## 6. Conclusion

We constructed bases for bicubic and biquartic  $C^1$ -smooth geometrically continuous isogeometric functions on bilinearly parameterized multi-patch domains  $\Omega \subset \mathbb{R}^2$ . The resulting basis functions are obtained by suitably combining the  $C^1$ -smooth functions from the two-patch case (cf. [16]) and can be easily generated by means of explicit formulas for their spline coefficients. We employed these basis functions to perform numerical experiments, which showed optimal rates of convergence. Our construction guarantees that polynomials of degree  $d$  on the physical domain are contained in the isogeometric discretization space, if the physical domain is bilinearly parameterized.

The paper leaves several open issues for possible future research. One such topic consists in the theoretical investigation of the approximation power of the space of  $C^1$ -smooth

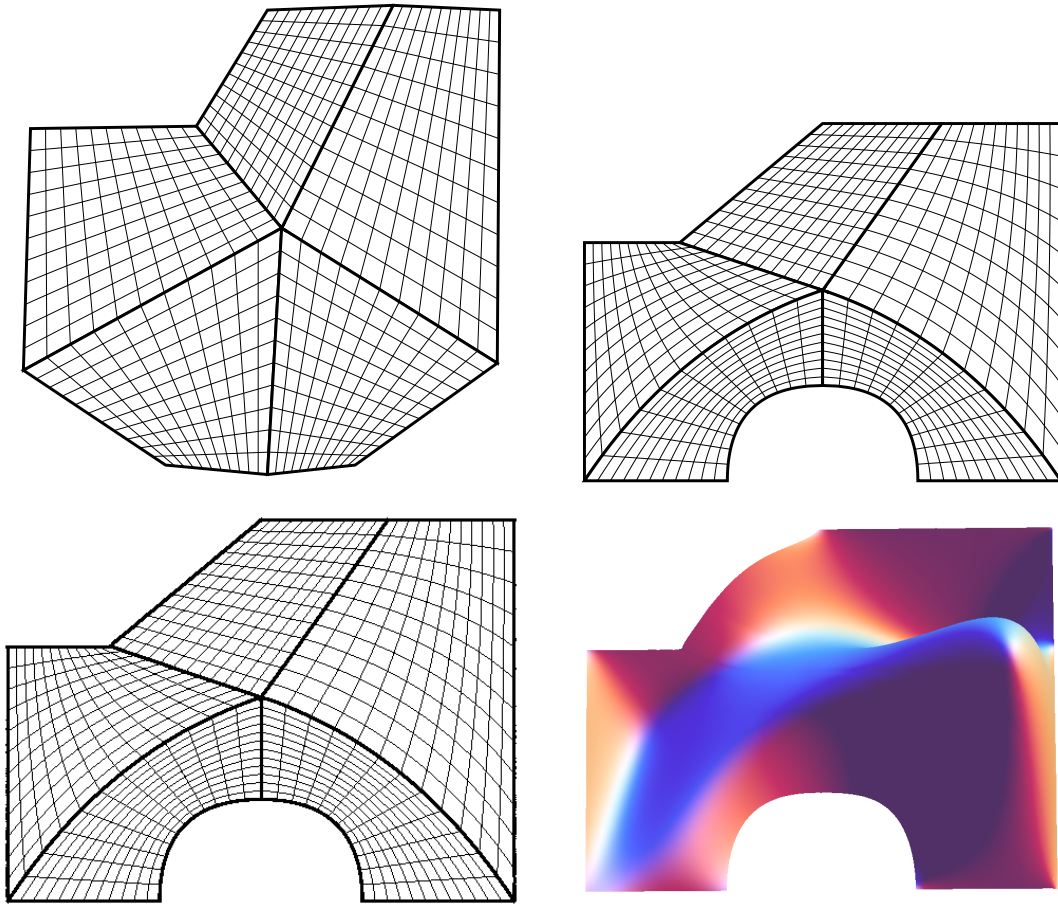


Figure 12: Solving Poisson's equation on a five-patch computational domain (bottom left) with the right side function  $f$  and Dirichlet boundary conditions obtained from the exact solution (38) (bottom right). The computational domain is constructed by performing  $L^2$  approximation with the help of a reference (top left) and target geometry (top right). See Exampe 6 and Table 2.

geometrically continuous isogeometric functions defined on bilinear multi-patch domains. First steps have been presented recently in [7] where necessary conditions (which are satisfied by our construction) for optimal approximation properties were identified.

Another challenging topic is the construction of geometrically continuous isogeometric functions of higher degree and/or global smoothness. In addition, the possibly finding of non-negative geometrically continuous isogeometric basis functions, satisfying the partition of unity property, would allow an interactive geometric design.

We have already demonstrated the potential of the geometrically continuous isogeometric functions by solving the biharmonic equation. The exploration of further possible applications, which require these functions of higher smoothness, is of interest, too. Finally, the extension of the framework to the three-dimensional case will be considered.

**Acknowledgment.** The authors wish to thank the anonymous reviewers for their comments that helped to improve the paper. This work was supported by the Austrian Science

## Appendix A. Setting of the multi-patch domains defined in Example 1

The coordinates of the vertices of the three multi-patch domains presented in Example 1, which are used for solving numerical problems in the Examples 2-4, are as follows:

- Three-patch domain:

$$\begin{aligned} \mathbf{v}_0 &= \left(-\frac{1}{10}, -\frac{3}{20}\right), & \mathbf{v}_1 &= \left(\frac{15}{4}, 2\right), & \mathbf{v}_2 &= \left(\frac{1}{20}, \frac{77}{20}\right), & \mathbf{v}_3 &= \left(-\frac{71}{20}, 2\right), \\ \mathbf{v}_4 &= \left(-\frac{13}{4}, -\frac{11}{5}\right), & \mathbf{v}_5 &= \left(-\frac{3}{20}, -\frac{19}{5}\right), & \mathbf{v}_6 &= \left(\frac{37}{10}, -\frac{37}{20}\right). \end{aligned} \quad (\text{A.1})$$

- Four patch domain:

$$\begin{aligned} \mathbf{v}_0 &= \left(-\frac{1}{5}, \frac{1}{5}\right), & \mathbf{v}_1 &= \left(\frac{21}{5}, -\frac{1}{5}\right), & \mathbf{v}_2 &= \left(\frac{37}{10}, \frac{7}{2}\right), \\ \mathbf{v}_3 &= \left(\frac{1}{5}, \frac{41}{10}\right), & \mathbf{v}_4 &= \left(-4, \frac{18}{5}\right), & \mathbf{v}_5 &= \left(-\frac{43}{10}, -\frac{1}{10}\right), \\ \mathbf{v}_6 &= \left(-\frac{39}{10}, -\frac{39}{10}\right), & \mathbf{v}_7 &= \left(\frac{3}{10}, -\frac{17}{4}\right), & \mathbf{v}_8 &= \left(\frac{39}{10}, -\frac{19}{5}\right). \end{aligned} \quad (\text{A.2})$$

- Five-patch domain:

$$\begin{aligned} \mathbf{v}_0 &= (0, 0), & \mathbf{v}_1 &= \left(\frac{24}{5}, 0\right), & \mathbf{v}_2 &= \left(\frac{9}{2}, \frac{32}{10}\right), & \mathbf{v}_3 &= \left(\frac{8}{5}, \frac{31}{10}\right), \\ \mathbf{v}_4 &= \left(-\frac{7}{10}, \frac{41}{10}\right), & \mathbf{v}_5 &= \left(-\frac{33}{10}, \frac{14}{5}\right), & \mathbf{v}_6 &= \left(-\frac{53}{10}, \frac{4}{5}\right), & \mathbf{v}_7 &= \left(-\frac{7}{2}, -\frac{9}{5}\right), \\ \mathbf{v}_8 &= \left(-3, -\frac{41}{10}\right), & \mathbf{v}_9 &= \left(\frac{4}{5}, -\frac{9}{2}\right), & \mathbf{v}_{10} &= \left(\frac{21}{5}, -\frac{27}{10}\right). \end{aligned} \quad (\text{A.3})$$

## Appendix B. Edge basis functions

We present simple explicit formulas for the spline coefficients of the different types of edge basis functions for bilinearly parameterized two-patch domains  $\Omega$ , see Section 3.2. Mathematica templates for computing these spline coefficients with respect to local geometries, described in the following paragraph, can be found under [http://www.ag.jku.at/pubs/Template\\_Degree3.nb](http://www.ag.jku.at/pubs/Template_Degree3.nb) and [http://www.ag.jku.at/pubs/Template\\_Degree4.nb](http://www.ag.jku.at/pubs/Template_Degree4.nb) for  $d = 3$  and  $d = 4$ , respectively.

*Local geometries.* The values  $b_i$  of their spline coefficients are specified with respect to local geometries of two, three or four pairs of adjacent elements along the common edge  $\Gamma^{(1,2)}$ , compare Fig.3, where the vertices

$$(0, 0), \left\{ \begin{array}{l} (0, 2) \\ (0, 3) \\ (0, 4) \end{array} \right\}, (x_0, y_0), (x_1, y_1), (x_2, y_2) \text{ and } (x_3, y_3)$$

are the vertices  $\mathbf{G}^{(\ell)}(\cdot, \cdot)$ ,  $\ell = 1, 2$ , of the involved bilinear elements in a suitably chosen local coordinate system. In addition, we assume that the functions of type L, U, and Y are constructed at the local vertex  $(0, 0)$ . To keep all formulas short and compact, we use the following abbreviations:

$$\tilde{d} = 5 - d, \quad \alpha_{i,j} = x_i y_j - x_j y_i, \quad \beta_{i,j} = x_j - x_i$$

and

$$\gamma_{i,j} = \alpha_{i,j} + \beta_{i,j}, \quad \delta_{i,j} = \alpha_{i,j} + 2\beta_{i,j}, \quad \varepsilon_{i,j} = \alpha_{i,j} + 3\beta_{i,j}, \quad \eta_{i,j} = \alpha_{i,j} + 4\beta_{i,j}$$

for  $i, j \in \{0, \dots, 3\}$  with  $i < j$ .

Basis functions of type A, B, L and U for  $d = 3$ .

- Type A:

$$\begin{aligned} b_6 &= \frac{x_0}{3x_2+2x_3}, b_8 = \frac{x_2}{3x_2+2x_3}, b_9 = \frac{3x_0+2x_1}{3x_2+2x_3}, b_{11} = 1, b_{12} = \frac{2x_0+3x_1}{3x_2+2x_3}, b_{14} = \frac{2x_2+3x_3}{3x_2+2x_3}, \\ b_{15} &= \frac{x_1}{3x_2+2x_3}, b_{17} = \frac{x_3}{3x_2+2x_3}. \end{aligned} \quad (\text{B.1})$$

- Type B:

$$\begin{aligned} b_8 &= \frac{\alpha_{0,2}}{12x_0}, b_9 = \frac{\alpha_{0,1}}{8x_0}, b_{10} = \frac{1}{2}, b_{11} = \frac{7\alpha_{0,2}+3\alpha_{0,3}}{24x_0}, \\ b_{12} &= \frac{3\alpha_{0,3}x_0+\alpha_{0,3}x_1+8\alpha_{0,1}x_3}{48x_0x_3} + \frac{3\beta_{0,3}+\beta_{1,3}}{12x_3}, b_{13} = 1, \\ b_{14} &= \frac{3\alpha_{0,3}x_2+8\alpha_{0,2}x_3+9\alpha_{0,3}x_3}{48x_0x_3} + \frac{\beta_{2,3}}{12x_3}, b_{15} = \frac{9\alpha_{0,3}x_0+11\alpha_{0,3}x_1-8\alpha_{0,1}x_3}{48x_0x_3} + \frac{9\beta_{0,3}+11\beta_{1,3}}{12x_3}, \\ b_{16} &= 1, b_{17} = \frac{9\alpha_{0,3}x_2-8\alpha_{0,2}x_3+3\alpha_{0,3}x_3}{48x_0x_3} + \frac{3\beta_{2,3}}{4x_3}, b_{18} = \frac{3\eta_{0,3}+7\eta_{1,3}}{24x_3}, b_{19} = \frac{1}{2}, \\ b_{20} &= \frac{\eta_{2,3}}{8x_3}, b_{21} = \frac{\eta_{1,3}}{12x_3}. \end{aligned} \quad (\text{B.2})$$

- Type L<sub>1</sub> and U<sub>1</sub>:

$$b_0 = \frac{2\gamma_{0,2}+\gamma_{0,3}}{2x_2+x_3}, b_1 = 1, b_2 = \frac{\gamma_{23}}{2x_2+x_3}, b_3 = \frac{4\gamma_{0,2}+2\gamma_{0,3}+2\gamma_{1,2}+\gamma_{1,3}}{18x_2+9x_3}. \quad (\text{B.3})$$

- Type L<sub>2</sub> and U<sub>2</sub>:

$$b_1 = 1, b_2 = -\frac{\gamma_{0,2}}{x_0}, b_3 = -\frac{\gamma_{0,1}}{9x_0}, b_5 = -\frac{2\gamma_{0,2}+\gamma_{0,3}}{9x_0}. \quad (\text{B.4})$$

- Type L<sub>3</sub> and U<sub>3</sub>:

$$\begin{aligned} b_2 &= \frac{\alpha_{0,2}}{x_0}, b_3 = \frac{\delta_{0,2}+2\delta_{0,3}}{3x_2+6x_3} + \frac{\alpha_{0,1}}{9x_0}, b_4 = 1, b_5 = \frac{-2\alpha_{0,2}\beta_{2,3}+7\alpha_{0,3}x_2+2\alpha_{0,3}x_3}{9x_0(x_2+2x_3)} + \frac{4\beta_{2,3}}{3x_2+6x_3}, \\ b_6 &= \frac{11\delta_{0,2}+22\delta_{0,3}+4\delta_{1,2}+8\delta_{1,3}}{36x_2+72x_3}, b_7 = \frac{1}{2}, b_8 = \frac{\delta_{2,3}}{2x_2+4x_3}, b_9 = \frac{\delta_{0,2}+2\delta_{0,3}+2\delta_{1,2}+4\delta_{1,3}}{36x_2+72x_3}. \end{aligned} \quad (\text{B.5})$$

- Type L<sub>4</sub> and U<sub>4</sub>:

$$b_3 = 1, b_5 = \frac{x_2}{x_0}, b_6 = \frac{11x_0+4x_1}{12x_0}, b_8 = \frac{11x_2+4x_3}{12x_0}, b_9 = \frac{x_0+2x_1}{12x_0}, b_{11} = \frac{x_2+2x_3}{12x_0}. \quad (\text{B.6})$$

- Type L<sub>5</sub> and U<sub>5</sub>:

$$\begin{aligned} b_5 &= \frac{2\alpha_{0,2}}{3x_0}, b_6 = \frac{2\alpha_{0,1}}{9x_0} + \frac{\varepsilon_{0,3}}{9x_3}, b_7 = 1, b_8 = \frac{2\alpha_{0,3}x_2+9\alpha_{0,2}x_3+4\alpha_{0,3}x_3}{18x_0x_3} + \frac{\beta_{2,3}}{3x_3}, \\ b_9 &= \frac{3\varepsilon_{0,3}x_0+2\varepsilon_{0,3}x_1-\varepsilon_{0,1}x_3}{9x_0x_3} - \frac{\beta_{0,1}}{3x_0}, b_{10} = \frac{4}{3}, b_{11} = \frac{6\alpha_{0,3}x_2-5\alpha_{0,2}x_3+2\alpha_{0,3}x_3}{18x_0x_3} + \frac{\beta_{2,3}}{x_3}, \\ b_{12} &= \frac{2\varepsilon_{0,3}+3\varepsilon_{1,3}}{9x_3}, b_{13} = \frac{2}{3}, b_{14} = \frac{2\varepsilon_{2,3}}{9x_3}, b_{15} = \frac{\varepsilon_{1,3}}{9x_3}. \end{aligned} \quad (\text{B.7})$$

Basis functions of type A, B, L and U for  $d = 4$ .

- Type A<sub>1</sub>:

$$b_6 = 1, b_8 = \frac{x_2}{x_0}, b_9 = 1 + \frac{3x_1}{4x_0}, b_{11} = \frac{4x_2+3x_3}{4x_0}, b_{12} = \frac{x_1}{4x_0}, b_{14} = \frac{x_3}{4x_0}. \quad (\text{B.8})$$

- Type A<sub>2</sub>:

$$\begin{aligned} b_8 &= \frac{\alpha_{0,2}}{2x_0}, b_9 = \frac{3\alpha_{0,1}}{8x_0} + \frac{\delta_{0,3}}{8x_3}, b_{10} = 1, b_{11} = \frac{\alpha_{0,3}x_2 + 3\alpha_{0,2}x_3 + 3\alpha_{0,3}x_3}{8x_0x_3} + \frac{\beta_{2,3}}{4x_3}, \\ b_{12} &= \frac{3\alpha_{0,3}x_0 + 4\alpha_{0,3}x_1 - 3\alpha_{0,1}x_3}{8x_0x_3} + \frac{3\beta_{0,3} + 4\beta_{1,3}}{4x_3}, b_{13} = 1, b_{14} = \frac{3\alpha_{0,3}x_2 - 3\alpha_{0,2}x_3 + \alpha_{0,3}x_3}{8x_0x_3} + \frac{3\beta_{2,3}}{4x_3}, \\ b_{15} &= \frac{\delta_{1,3}}{2x_3}. \end{aligned} \quad (\text{B.9})$$

- Type A<sub>3</sub>:

$$b_9 = \frac{x_0}{4x_3}, b_{11} = \frac{x_2}{4x_3}, b_{12} = \frac{3x_0 + 4x_1}{4x_3}, b_{14} = 1 + \frac{3x_2}{4x_3}, b_{15} = \frac{x_1}{x_3}, b_{17} = 1. \quad (\text{B.10})$$

- Type B:

$$\begin{aligned} b_{11} &= \frac{\alpha_{0,2}}{16x_0}, b_{12} = \frac{\alpha_{0,1}}{6x_0}, b_{13} = \frac{1}{2}, b_{14} = \frac{13\alpha_{0,2} + 8\alpha_{0,3}}{48x_0}, b_{15} = \frac{\varepsilon_{0,3}(2x_0 + x_1) + \varepsilon_{0,1}x_3}{12x_0x_3} - \frac{\beta_{0,1}}{2x_0}, \\ b_{16} &= 1, b_{17} = \frac{2\varepsilon_{0,3}(x_2 + x_3) - \varepsilon_{0,2}x_3}{12x_0x_3} - \frac{\beta_{0,2} + 2\beta_{0,3}}{4x_0}, b_{18} = \frac{8\varepsilon_{0,3} + 13\varepsilon_{1,3}}{48x_3}, b_{19} = \frac{1}{2}, b_{20} = \frac{\varepsilon_{2,3}}{6x_3}, \\ b_{21} &= \frac{\varepsilon_{1,3}}{16x_3}. \end{aligned} \quad (\text{B.11})$$

- Type L<sub>1</sub> and U<sub>1</sub>:

$$b_0 = \frac{\gamma_{0,2} + \gamma_{0,3}}{x_2 + x_3}, b_1 = 1, b_2 = \frac{\gamma_{2,3}}{x_2 + x_3}, b_3 = \frac{\gamma_{0,2} + \gamma_{0,3} + \gamma_{1,2} + \gamma_{1,3}}{8x_2 + 8x_3}. \quad (\text{B.12})$$

- Type L<sub>2</sub> and U<sub>2</sub>:

$$b_1 = 1, b_2 = -\frac{\gamma_{0,2}}{x_0}, b_3 = -\frac{\gamma_{0,1}}{8x_0}, b_5 = -\frac{\gamma_{0,2} + \gamma_{0,3}}{8x_0}. \quad (\text{B.13})$$

- Type L<sub>3</sub> and U<sub>3</sub>:

$$\begin{aligned} b_2 &= \frac{\alpha_{0,2}}{x_0}, b_3 = \frac{6\gamma_{0,2}x_0 + 6\gamma_{0,3}x_0 + \alpha_{0,1}(x_2 + x_3)}{8x_0x_2 + 8x_0x_3}, b_4 = 1, \\ b_5 &= \frac{\alpha_{0,2}x_2 + 7\alpha_{0,3}x_2 - 5\alpha_{0,2}x_3 + \alpha_{0,3}x_3}{8x_0x_2 + 8x_0x_3} + \frac{3\beta_{2,3}}{4x_2 + 4x_3}, b_6 = \frac{\gamma_{0,2} + \gamma_{0,3} + \gamma_{1,2} + \gamma_{1,3}}{4x_2 + 4x_3}. \end{aligned} \quad (\text{B.14})$$

- Type L<sub>4</sub> and U<sub>4</sub>:

$$b_3 = 1, b_5 = \frac{x_2}{x_0}, b_6 = \frac{x_0 + x_1}{3x_0}, b_8 = \frac{x_2 + x_3}{3x_0}. \quad (\text{B.15})$$

- Type L<sub>5</sub> and U<sub>5</sub>:

$$\begin{aligned} b_5 &= \frac{3\alpha_{0,2}}{4x_0}, b_6 = \frac{\alpha_{0,1}}{4x_0} + \frac{\delta_{0,3}}{4x_3}, b_7 = 1, b_8 = \frac{2x_0\beta_{2,3} + \alpha_{0,3}(x_2 + x_3)}{4x_0x_3}, b_9 = \frac{4\delta_{0,3} + 3\delta_{1,3}}{16x_3}, \\ b_{10} &= \frac{1}{2}, b_{11} = \frac{\delta_{2,3}}{4x_3}, b_{12} = \frac{\delta_{1,3}}{16x_3}. \end{aligned} \quad (\text{B.16})$$

*Basis functions of type Y.* The functions of type Y are obtained by linearly combining the functions of type L, i.e.

$$Y_i = \sum_{j=1}^5 \mu_j^i L_j, \quad i = 1, \dots, 5,$$

using the following coefficients  $\mu_j^i$ :

- type  $Y_1$ :

$$\begin{aligned}\mu_1^1 &= \frac{\tilde{d}x_2+x_3}{\tilde{d}\gamma_{0,2}+\gamma_{0,3}}, \mu_2^1 = \frac{\tilde{d}(\gamma_{0,2}-x_2)+\gamma_{0,3}-x_3}{\tilde{d}\gamma_{0,2}+\gamma_{0,3}}, \mu_3^1 = 1, \\ \mu_4^1 &= -\frac{(2d-5)\alpha_{0,2}+(d-1)\alpha_{0,3}+d\beta_{0,2}-(6-d)x_0+(12-2d)x_3}{dx_2+(12-2d)x_3}, \mu_5^1 = \frac{(2d-5)\alpha_{0,2}+d\beta_{0,2}}{(d-1)\alpha_{0,2}}.\end{aligned}\tag{B.17}$$

- type  $Y_2$ :

$$\begin{aligned}\mu_1^2 &= \frac{(\tilde{d}x_2+x_3)(x_0 \cos \varphi+y_0 \sin \varphi)}{(12-2d)\gamma_{0,2}+d\gamma_{0,3}}, \mu_2^2 = -\frac{(\tilde{d}x_2+x_3)(x_0 \cos \varphi+y_0 \sin \varphi)}{(12-2d)\gamma_{0,2}+d\gamma_{0,3}}, \mu_3^2 = \frac{\sin \varphi}{d}, \\ \mu_4^2 &= -\frac{(\tilde{d}x_0+x_1)(x_2+\tilde{d}x_3) \cos \varphi+(-(x_2+\tilde{d}x_3)(-6+(4d-11)y_0-y_1)+(3d-6)x_0((4d-18)+y_2+\tilde{d}y_3)) \sin \varphi}{(5d+12)x_2+(120-22d)x_3}, \\ \mu_5^2 &= \frac{(-x_1x_2+x_0x_3) \cos \varphi+x_2(-6+(4d-11)y_0-y_1)+x_0(6-(4d-11)y_2+y_3) \sin \varphi}{6d\alpha_{0,2}}.\end{aligned}\tag{B.18}$$

- type  $Y_3$ :

$$\begin{aligned}\mu_1^3 &= \frac{(\tilde{d}x_2+x_3)(y_0 \cos \varphi-x_0 \sin \varphi)}{(12-2d)\gamma_{0,2}+d\gamma_{0,3}}, \mu_2^3 = -\frac{(\tilde{d}x_2+x_3)(y_0 \cos \varphi-x_0 \sin \varphi)}{(12-2d)\gamma_{0,2}+d\gamma_{0,3}}, \mu_3^3 = \frac{\cos \varphi}{d}, \\ \mu_4^3 &= -\frac{-(\tilde{d}x_0+x_1)(x_2+\tilde{d}x_3) \sin \varphi+(-(x_2+\tilde{d}x_3)(-6+(4d-11)y_0-y_1)+(3d-6)x_0((4d-18)+y_2+\tilde{d}y_3)) \cos \varphi}{(5d+12)x_2+(120-22d)x_3}, \\ \mu_5^3 &= \frac{(x_1x_2-x_0x_3) \sin \varphi+(x_2(-6+(4d-11)y_0-y_1)+x_0(6-(4d-11)y_2+y_3)) \cos \varphi}{6d\alpha_{0,2}}.\end{aligned}\tag{B.19}$$

- type  $Y_4$ :

$$\mu_1^4 = 0, \mu_2^4 = 0, \mu_3^4 = 0, \mu_4^4 = 1, \mu_5^4 = -\frac{dx_2}{(d-1)\alpha_{0,2}}.\tag{B.20}$$

- type  $Y_5$ :

$$\mu_1^5 = 0, \mu_2^5 = 0, \mu_3^5 = 0, \mu_4^5 = 0, \mu_5^5 = \frac{dx_0}{(d-1)\alpha_{0,2}}.\tag{B.21}$$

Note, that  $\varphi$  is the angle between the vector  $(1, 0)$  and the directional vector of the common edge  $\Gamma^{(1,2)}$  with respect to global coordinates.

## References

- [1] A. Apostolatos, R. Schmidt, R. Wüchner, and K.-U. Bletzinger. A Nitsche-type formulation and comparison of the most common domain decomposition methods in isogeometric analysis. *Int. J. Numer. Methods Engrg.*, 97(7):473–504, 2014.
- [2] M. Bercovier and T. Matskewich. Smooth Bézier surfaces over arbitrary quadrilateral meshes. Technical Report 1412.1125, arXiv.org, 2014.
- [3] E. Brivadis, A. Buffa, B. Wohlmuth, and L. Wunderlich. Isogeometric mortar methods. *Comp. Methods Appl. Mech. Engrg.*, 284:292–319, 2015.
- [4] A. M. Bruaset. *A survey of preconditioned iterative methods*, volume 328 of *Pitman Research Notes in Mathematics Series*. Longman Scientific & Technical, Harlow, 1995.
- [5] F. Buchegger, B. Jüttler, and A. Mantzaflaris. Adaptively refined multi-patch B-splines with enhanced smoothness. *Applied Mathematics and Computation*, 272:159 – 172, 2016.

- [6] Philippe G. Ciarlet. *The finite element method for elliptic problems*. North-Holland Publishing Co., Amsterdam-New York-Oxford, 1978. Studies in Mathematics and its Applications, Vol. 4.
- [7] A. Collin, G. Sangalli, and T. Takacs. Approximation properties of multi-patch  $C^1$  isogeometric spaces. Technical Report 1509.07619, arXiv.org, 2015.
- [8] J. A. Cottrell, T.J.R. Hughes, and Y. Bazilevs. *Isogeometric Analysis: Toward Integration of CAD and FEA*. John Wiley & Sons, Chichester, England, 2009.
- [9] W. Dornisch, G. Vitucci, and S. Klinkel. The weak substitution method—An application of the mortar method for patch coupling in NURBS-based isogeometric analysis. *Int. J. Numer. Methods Engrg.*, 103(3):205–234, 2015.
- [10] G. Farin. *Curves and Surfaces for Computer-Aided Geometric Design*. Academic Press, 1997.
- [11] D. Groisser and J. Peters. Matched  $G^k$ -constructions always yield  $C^k$ -continuous isogeometric elements. *Computer Aided Geometric Design*, 34:67 – 72, 2015.
- [12] C. Hesch and P. Betsch. Isogeometric analysis and domain decomposition methods. *Comput. Methods Appl. Mech. Engrg.*, 213/216:104–112, 2012.
- [13] C. Hofer and U. Langer. Dual-primal isogeometric tearing and interconnecting solvers for large-scale systems of multipatch continuous Galerkin IgA equations. Technical Report 39, NFN Geometry + Simulation, Johannes Kepler University, Linz/Austria, 2015. [www.gs.jku.at](http://www.gs.jku.at).
- [14] J. Hoschek and D. Lasser. *Fundamentals of computer aided geometric design*. A K Peters Ltd., Wellesley, MA, 1993.
- [15] T. J. R. Hughes, J. A. Cottrell, and Y. Bazilevs. Isogeometric analysis: CAD, finite elements, NURBS, exact geometry and mesh refinement. *Comput. Methods Appl. Mech. Engrg.*, 194(39-41):4135–4195, 2005.
- [16] M. Kapl, V. Vitrih, B. Jüttler, and K. Birner. Isogeometric analysis with geometrically continuous functions on two-patch geometries. *Comput. Math. Appl.*, 70(7):1518 – 1538, 2015.
- [17] K. Karčiauskas, T. Nguyen, and J. Peters. Generalizing bicubic splines for modeling and IGA with irregular layout. *Computer-Aided Design*, 70:23 – 35, 2016.
- [18] S. Kleiss, C. Pechstein, B. Jüttler, and S. Tomar. IETI – isogeometric tearing and interconnecting. *Computer Methods in Applied Mechanics and Engineering*, 247-248:201–215, 2012.
- [19] M.-J. Lai and L. L. Schumaker. *Spline functions on triangulations*, volume 110 of *Encyclopedia of Mathematics and its Applications*. Cambridge University Press, Cambridge, 2007.
- [20] U. Langer, A. Mantzaflaris, S.E. Moore, and I. Touloupoulos. Multipatch discontinuous Galerkin isogeometric analysis. In B. Jüttler and B. Simeon, editors, *Isogeometric Analysis and Applications 2014*, LNCSE. Springer, 2015. in press, also available at arXiv:1505.03505.
- [21] T. Nguyen, K. Karčiauskas, and J. Peters. A comparative study of several classical, discrete differential and isogeometric methods for solving poisson’s equation on the disk. *Axioms*, 3(2):280–299, 2014.
- [22] T. Nguyen, K. Karčiauskas, and J. Peters.  $C^1$  finite elements on non-tensor-product 2d and 3d manifolds. *Applied Mathematics and Computation*, 272:148 – 158, 2016.
- [23] V.P. Nguyen, P. Kerfriden, M. Brino, S.P.A. Bordas, and E. Bonisoli. Nitsche’s method for two and three dimensional NURBS patch coupling. *Comput. Mech.*, 53(6):1163–1182, 2014.

- [24] J. Peters. Geometric continuity. In *Handbook of computer aided geometric design*, pages 193–227. North-Holland, Amsterdam, 2002.
- [25] M.A. Scott, R.N. Simpson, J.A. Evans, S. Lipton, S.P.A. Bordas, T.J.R. Hughes, and T.W. Sederberg. Isogeometric boundary element analysis using unstructured t-splines. *Comp. Methods Appl. Mech. Engrg.*, 254:197 – 221, 2013.
- [26] M.A. Scott, D.C. Thomas, and E.J. Evans. Isogeometric spline forests. *Comp. Methods Appl. Mech. Engrg.*, 269:222–264, 2014.
- [27] F. Zhang, Y. Xu, and F. Chen. Discontinuous Galerkin methods for isogeometric analysis for elliptic equations on surfaces. *Commun. Math. Stat.*, 2(3-4):431–461, 2014.